UNIVERSIDADE FEDERAL DE SANTA CATARINA
PROGRAMA DE PÓS-GRADUAÇÃO EM CIÊNCIA E ENGENHARIA DE MATERIAIS

João Gustavo Pereira da Silva

MODELING OF LOAD TRANSFER IN CERAMIC MATRIX COMPOSITES

Dissertação submetida ao Programa de Pós Graduação em Ciência e Engenharia de Materiais da Universidade Federal de Santa Catarina para a obtenção do Grau de Mestre em Ciência e Engenharia de Materiais
Orientador: Prof. Hazim Ali Al-Qureshi, PhD.
Co-orientador: Prof. Dachamir Hotza, Dr. Ing.

Florianópolis

2011

João Gustavo Pereira da Silva

MODELING OF LOAD TRANSFER IN CERAMIC MATRIX COMPOSITES

Esta Dissertação foi julgada adequada para obtenção do Título de Mestre em Ciência e Engenharia de Materiais, e aprovada em sua forma final pelo Programa de Pós Graduação em Ciência e Engenharia de Materiais

Florianópolis, 26 de Agosto de 2011.

____

Prof. Carlos Augusto Silva de Oliveira, Dr.
Coordenador do Curso

Banca Examinadora:

____

Prof. Hazim Ali Al-Qureshi, Ph.D,
Orientador
UFSC – CEM/EMC

____

Prof. Dachamir Hotza, Dr. Ing,
Co-Orientador
UFSC – EQA

____

Prof. Guilherme Mariz de Oliveira Barra, Dr,
UFSC – EMC

____

Prof. Márcio Celso Fredel, Dr. Ing,
UFSC - EMC

____

Prof. Carlos Pérez Bergmann, Dr.Ing,
Membro Externo
UFRGS - DEM

ACKNOWLEDGMENTS

First of all, I would like to thank the Universidade Federal de Santa Catarina in the name of all of the people who contributed in my learning experience here.

To the Graduate Program in Materials Science and Engineering coordinators, professors and workers.

To the funding agencies, CAPES and DFG, for the scholarships inland and abroad.

To my master and advisor Prof. Hazim Ali Al-Qureshi, who “infected” me with this blessing that is to think always in the ways of mathematics.

To Prof. Dachamir Hotza, co-advisor, for all the insights and project support, as well as for the opportunity to spend a year in Hamburg.

To the Hamburg University of Technology (TUHH), namely for the Institute of Advanced Ceramics, in the person of Prof. Schneider.

To Dr. Rolf Janssen, my supervisor during my stay in Hamburg. Thanks for the discussions about the work and the motivation for the bundle simulation part.

To the staff and fellow students during my time at TUHH: Anja, Manfred, Paula, Rodrigo, Lucas, Gabriel, Hüssein, Wolfgang, Sascha, Nils, Ezgi, Nicole, Tobias, and others, thanks for the good times in Hamburg.

To Peter Gührs and Henrik Schmützler, from the THF for the help with the fiber testing.

To my fellows in Cermat, for the support and helpful discussions.

To my dear Clara, for all the support and tenderness even in the darkest hours;

To my family, for all my education and love, shared without measures.

All Models are wrong, but some are useful.

(George E.P. Box)

ABSTRACT

The aim of this work is to present some models of load transfer between porous matrix and fibers in ceramic matrix composites. An analytical model for short fibers is developed, based on the earlier shear-lag models used for polymeric composites. Moreover, geometry and strength of fibers in addition to the matrix porosity are included in the present analysis. The theoretical curves for the longitudinal and shear stress distribution along the fiber-porous matrix interface are presented. They exhibited a maximum strength point at the middle of the short fibers. It became evident that the critical length is governed by the relative properties of the fibers, matrix and porosity, which greatly influenced the load carrying capacity of the fibers in the composites. In addition, the present simplified solution facilitates the understanding of the interface mechanism using porous matrix. In addition, a bundle testing routine is implemented using Monte Carlo methods. It is common knowledge that for bundles of fibers in composites, that the bundle strength is always less than the sum of the fiber strengths. This behavior can be explained by load-sharing models. At this work, different load sharing models were implemented on a simulated tensile test of ceramic oxide fibers. The results are in agreement with the experimental results of single-fiber and bundle testing and constitute a useful tool for the design of fiber-reinforced materials.

Keywords: modeling, load transfer, ceramic matrix composites

RESUMO

Este trabalho se dedica a apresentar alguns modelos de transferência de carga entre uma matriz porosa e fibras em compósitos de matriz cerâmica. Um modelo analítico para a transferência de carga em fibras curtas é desenvolvido, baseado em modelos já existentes para compósitos poliméricos. Além disso, a geometria e a resistência das fibras, juntamente com a porosidade da matriz são incluídas na presente análise. As curvas teóricas para as tensões longitudinais e de cisalhamento ao longo da interface fibra-matriz são apresentadas. Elas alcançam um máximo no meio das fibras curtas. Torna-se evidente que o comprimento crítico é governado pelo conjunto de propriedades da fibra e da matriz, que influenciam a capacidade de transferência de carga nos compósitos. Adicionalmente, a solução simplificada apresentada facilita o entendimento dos mecanismos interfaciais se utilizando de uma matriz porosa. Outro foco do trabalho é um algoritmo que simula o teste de feixes contínuos de fibras cerâmicas usando-se métodos de Monte Carlo. É mostrado que a resistência do feixe é sempre menor que a resistência média das fibras testadas individualmente. Tal comportamento é explicado por modelos de transferência de carga. Neste trabalho, diferentes modelos de transferência de carga foram implementados em uma simulação de um ensaio de tração em feixes de fibras. Os resultados estão de acordo com os experimentos de fibra simples e feixe realizados e constituem uma ferramenta útil para o projeto de materiais reforçados com fibras cerâmicas.

Palavras-chave: modelamento, transferência de carga, compósitos de matriz cerâmica.

FIGURE INDEX

TABLE INDEX

ABBREVIATIONS AND ACRONYMS LIST

CMCs – Ceramic Matrix Composites
SiC – Silicon Carbide
$LaPO_4$ - Monazite
ELS – Equal Load Sharing
LLS – Local Load Sharing

SYMBOL LIST

$F(\sigma)$ – Failure probability of a single fiber at a stress σ
$G_b(\sigma)$ – Failure probability of a dry fiber bundle at a stress σ
$G_i(\sigma)$ – Failure probability of an infiltrated fiber bundle at a stress σ
$G_c(\sigma)$ – Failure probability of a fiber bundle within a composite at a stress σ
α – Dunders parameter, Critical length ratio
E_m – Matrix Young's modulus
E_f – Fiber Young's modulus
G_d – Energy release rate for crack deflection in an interface
G_p – Energy release rate for crack penetration in an interface
Γ_i – Interfacial toughness
Γ_m – Matrix toughness (work of fracture)
Σ – Crack deflection parameter
L – Half of a fiber's length
r – Fiber radius
u – Displacement on the fiber
v – Displacement on the matrix
σ - Stress
E – Young's modulus
ε - Strain
P_f – Load on the fiber
B – Cox's proportionality constant
m – Weibull Modulus
σ_0 – Characteristic strength (F=0.632) for a Weibull distribution
K_i – i-th load concentration factor for i broken neighbors
k* – Critical cluster size
b – Sintering parameter
v_f – Fiber volume fraction
σ_f – Fiber rupture stress
σ_m – Matrix rupture stress
σ_T – Composite transversal strength
σ_L – Composite longitudinal strength

TABLE OF CONTENTS

1 INTRODUCTION

Modern structural ceramic composites possess a number of unique properties that cannot be achieved by other materials. Therefore, they have a potential for saving energy, reducing wear, and increasing the lifetime of components [1].

Ceramic Matrix Composites (CMCs) have attracted attention for thermomechanical applications, due to their damage tolerant fracture behavior. This is the result of toughening mechanisms, particularly crack deflection into fiber-matrix interface, as well as subsequent fiber pullout and bridging [2, 3]. Among the different categories of CMCs, all-oxide systems have recently been in the focus of research [4-9] because of their inherent high oxidation resistance compared to their non-oxide counterparts. This is interesting particularly at high temperature applications in oxidizing environments such as gas turbines.

Due to the complexity and responsibility of these materials, there is a growing need to models which can predict the bulk properties of the composite based on their microconstituents, e.g. fiber and matrix properties. This leads to micromechanical modeling (Fig. 1.1), which is an idealization of the interaction of the fibers and the matrix on the microscale.

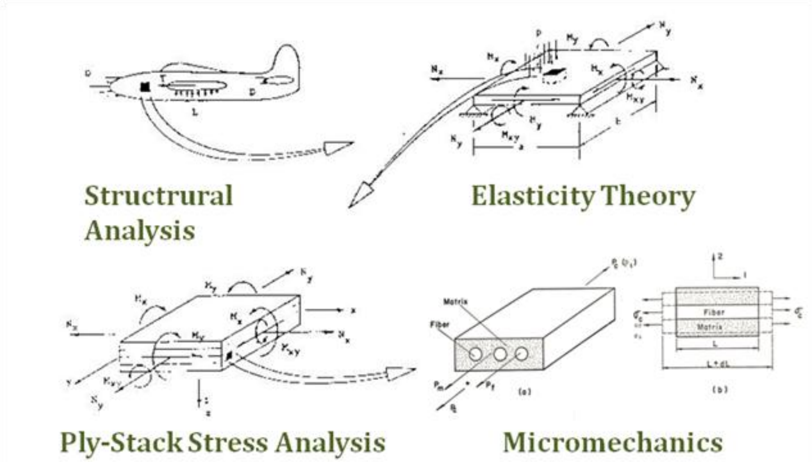

Fig. 1.1 Top-bottom approach for micromechanical modeling. Adapted from: [10] and [11]

The philosophy of this thesis is based on the recognition that mechanism-based models are needed, which allow for an efficient correlation to a well-conceived experimental procedure. The emphasis here is on the creation of a framework which allows models to be inserted in different complexity levels (Fig. 1.2), as they are developed, and which can also be validated by carefully chosen experiments.

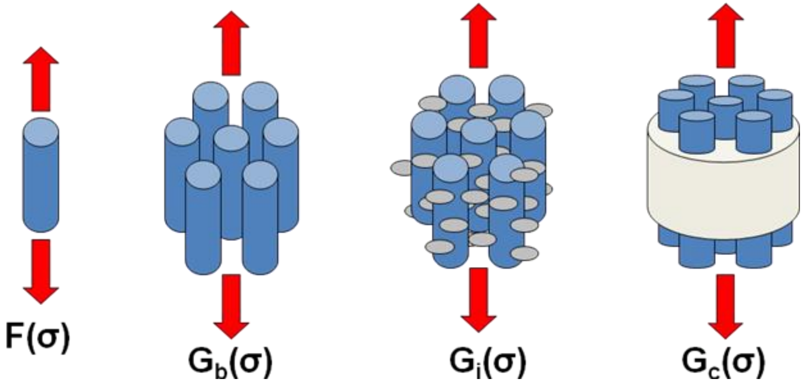

Fig. 1.2 Different complexity levels on a continuous fiber composite, each corresponding a failure probability function. From left to right: Single Fiber, Dry Bundle, Infiltrated Bundle and Consolidated Composite.

1.1 OBJECTIVES

This work has the main objective of understanding and modeling the mechanical behavior of ceramic matrix composites and fiber bundles, and the influence of processing and the matrix material in the mechanical behavior of the referred materials.
To achieve this goal, the following objectives were set:

- Develop a simplified shear-lag model for short-fiber ceramic matrix composites;
- Relate single-fiber properties and bundle properties;
- Simulate diverse load-sharing models for fiber bundles and determine the best suited for the studied ceramic fibers;

2 LITERATURE REVIEW

2.1 CERAMIC FIBERS

The high potential of CMCs is directly related to the use of high-resistance ceramic fibers of small diameters (usually around 10 μm). Covalent non-oxide fibers, as carbon or silicon carbide, are the ones showing better high-temperature mechanical properties (specially in terms of creep resistance), but are highly susceptible to oxidizing environments, calling to the use of surface treatments for protection, or the use of inert atmospheres [12].

In the other end of the spectrum, oxide fibers (as alumina and mullite-alumina), by their chemical nature, show an excellent oxidation resistance, good mechanical properties at room temperature, but present issues with creep resistance even in moderate temperatures. As consequence, the carbon and SiC fibers are the most used as reinforcement in commercial high-temperature CMCs [13].

By their small diameters, those ceramic fibers are extremely fragile and should be put into a ceramic matrix (either oxide or non-oxide), in a manner to protect them and permit the load transfer between the matrix and the fibers. The high cost of these composites is related to the high cost of those fibers, which are used in volumetric fractions ranging from 40% to 50%. Nanometric reinforcements, as carbon nanotubes, SiC nanofibers or whiskers, are not used in CMCs due to processing difficulties, cost and health hazards [12].

2.1.1 Oxide Ceramic Fibers

Nextel 610 and 720 are denominations amongst a group of aluminum oxide fibers specifically designed for use as reinforcement in ceramic and metal matrix composites. Both continuous fibers are designed as composite reinforcements, but their compositional differences result in differing properties. Nextel 610 was designed to have higher strength characteristics but is susceptible to creep at elevated temperatures. Nextel 720 was then designed to have better creep resistance for elevated temperature applications, but was reduced in strength. The Nextel fibers are mostly comprised of alumina, produced via sol-gel processing, which in turn makes them less expensive to produce than some other fibers, such as SiC.

The high strength of Nextel fibers is one of its primary characteristics that make it appealing as reinforcement for composites. Their high strength is attributed in part to the fine grain structure of the material that is achieved through careful control of the processing technique. Nextel 610 fibers are comprised almost entirely of a pure α-Alumina, and the Nextel 720 possess mullite specially placed on the grain boundaries. Through proper use of nucleation agents and careful control during processing, Nextel fibers are produced with a uniform microstructure comprised of grains 0.1 μm in size and little residual porosity [12].

Table 2.1. Nextel 610 and 720 fiber properties [12].

Property	Nextel 610	Nextel 720
Composition	Alumina	Alumina + Mullite
Weibull Modulus (m)	11.4	8
Characteristic Strength (MPa)	3200	2200
Mean Diameter (μm)	10	10

2.2 MECHANICAL PROPERTIES

The mechanical properties of ceramic matrix composites have not been studied until the 1990’s [2, 14-18]. Extensive reviews of mechanisms and mechanical properties of ceramic matrix composites are found in the literature [19, 20]. The main topics studied are dense and porous matrix composites.

For a dense-matrix composite (porosity higher than 90%), a surface treatment on the fibers is needed for crack deflection [21]. The development of oxide-oxide composites is based in a fragile fiber/matrix interface for crack deflection, giving place to oxidation-resistant coatings which are chemically stable. Monazite ($LaPO_4$), hibonite and scheelite are among the various materials studied. Morgan et al. [22] and Chawla et al. [23] have shown that due to the chemical compatibility of monazite with alumina at high temperatures, this coating would be a good candidate for an interface material in alumina-based composites. Since that time, numerous manufacturing trials of monazite films and its use with different combinations of matrix and fibers were investigated

[24, 25]. The degradation of fiber resistance caused by the film and the need for expensive thermal treatments were identified as barriers to the application of these materials [25].

It was shown also that a similar behavior in relation to crack deflection can be achieved by the means of a finely distributed porosity in the matrix instead of a separate interface between matrix and fibers [14].

For a highly porous matrix, the main objective is to insulate the fibers from cracks that can start on the matrix. Due to the highly porous matrix material, the energy is dissipated and the stress concentration around the fibers is reduced. The crack propagation for the neighboring fibers is inhibited and the same are intact even with the matrix fracture (Fig. 2.1) [26].

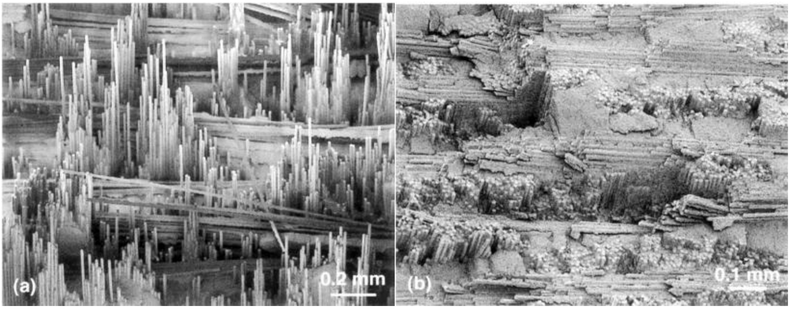

Fig. 2.1 Fracture surface of ceramic composites, showing: a) high-porosity matrix and b) low porosity matrix [14].

Although the matrix rules the pullout and crack deflection phenomena, the mechanical properties of the composite are strongly dependant of the fibers used as reinforcement. For composites with a volumetric fraction between 0.35 and 0.4, the typical values are of an elasticity modulus between 60 and 110 GPa and a bending strength between 140 and 220 MPa [14]. The higher values are from alumina fiber-reinforced composites (Nextel 610) and the lower from alumina-mullite fibers (Nextel 720).

This porous matrices are usually produced by pressure infiltration of slurries (Fig. 2.2) in a perform with the fibers, followed by drying and sintering [16, 27-29].

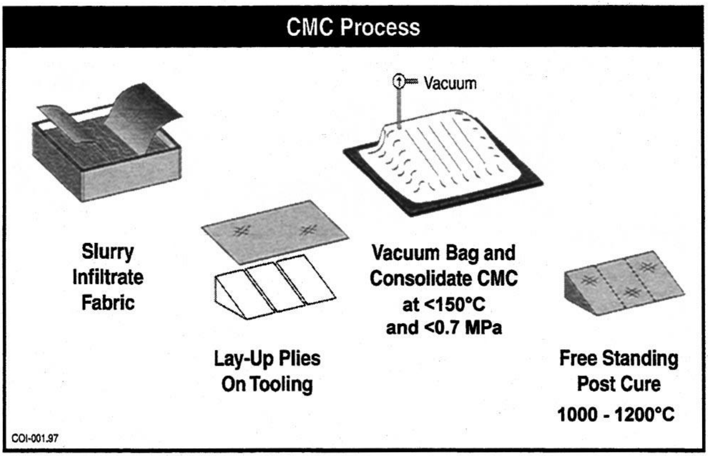

Fig 2.2 CMC production by slurry infiltration [14].

2.2.1 Damage Tolerance in Ceramic Composites

The damage tolerance in composite materials is thoroughly attributed to the crack deflection phenomenon between matrix and fiber (Fig. 2.3). The toughening occurs by the microcracking of the matrix and crack deflection, which keeps the fiber structure intact until the material fracture.

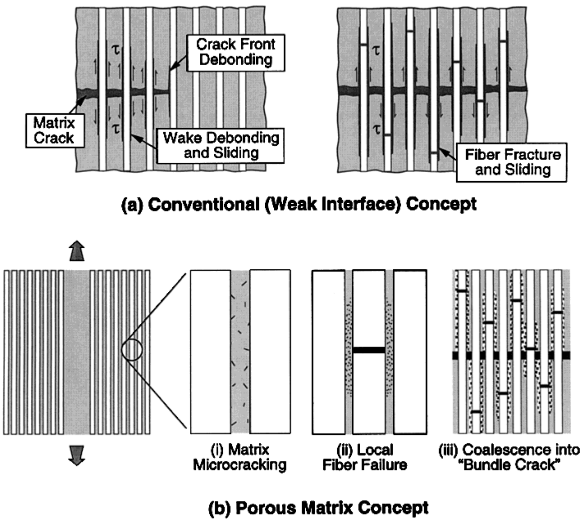

Fig. 2.3 Crack deflection phenomena in: a) dense matrix composite with weak interface and b) porous matrix composite [20].

The crack-deflection phenomena in two different materials of different elastic modulus were studied by He and Hutchinson [30]. One important variable to be considered is the Dunders parameter (α), which is a measure of the mismatch between the elastic modulus of matrix (E_m) and fiber (E_f):

$$\alpha = \frac{(E_f - E_m)}{(E_f + E_m)} \tag{2.1}$$

When using an energy balance, it is noted that the ratio between the energy release rate when the crack propagate between the interface G_d and the energy release rate on crack penetration G_p should be equal to the ratio of the interfacial toughness between interface and matrix [30] (eq 2.2):

$$\frac{G_d}{G_p} = \frac{\Gamma_i}{\Gamma_m} \tag{2.2}$$

A semiempiric relationship for G_d/G_p is given by Fujita et al. [27]:

$$\frac{G_d}{G_p} = \frac{1}{4(1-\alpha)^{0,9}} \tag{2.3}$$

The graphical representation of this criterion is given by Fig. 2.4, showing where the usual porous ceramic matrix composites can be found.

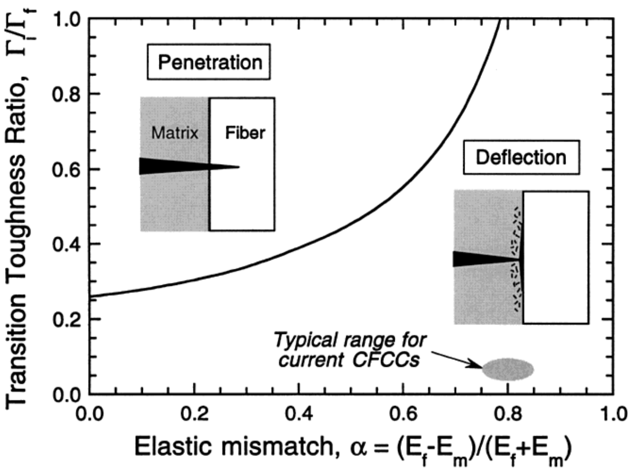

Fig. 2.4 He-Hutchinson criteria for crack deflection [20].

Replacing (2.1) in (2.3) and assuming $\Gamma_i = \Gamma_f$:

$$\Sigma = 0{,}134\left(\frac{\Gamma_f}{\Gamma_m}\right)\left(1+\frac{E_f}{E_m}\right)^{0{,}9} \tag{2.4}$$

where Σ is a non-dimensional parameter which represent the propensity for crack deflection for values higher than 1. So, by knowing the relationship between the elasticity modulus between matrix and fiber, their interfacial toughness and their evolution, it is possible to predict their behavior in service and the optimal sintering parameters.

Using those criteria, Fujita et al. [27] have determined the service time of mullite-alumina composites, reinforced with Nextel 720 fibers. A model to predict the evolution of matrix properties in relation to the time was developed (Fig. 2.5):

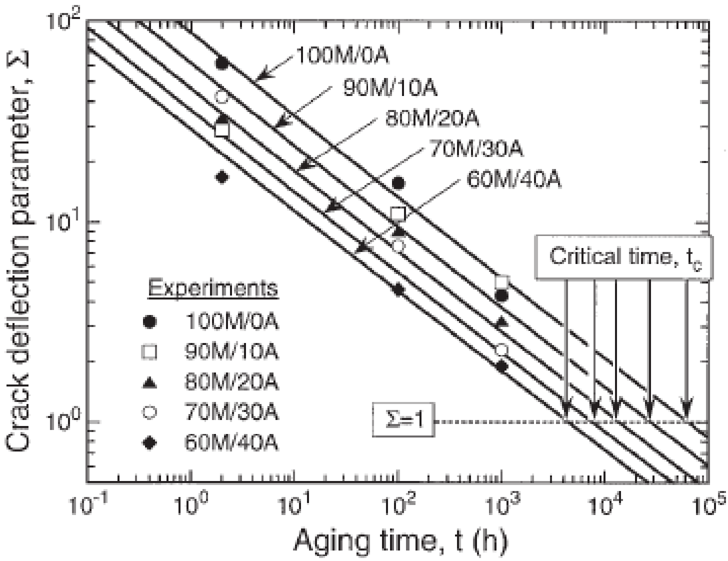

Fig 2.5 Evolution of Σ with sintering time [27].

The indexes denote the matrix composition. 100M/0A would be a composite with 100% mullite and 0% alumina, and so on. Composites with a higher mullite content show a better service time, what can be explained by the lower mullite sinterability [27].

2.2.2 Load transfer in short fiber composites

As a pioneer model for load transfer in short-fiber reinforced composites, Cox [31] published a shear-lag model to predict the strength of paper (which is indeed a composite of cellulose and lignin fibers). The model is explained briefly in the next section:

A loaded composite made of a dense fiber with length 2L is embedded in a porous matrix made of the same material as the fiber, as shown in Fig.1. It is assumed that no slippage occurs between fiber and matrix. It should also be considered that the Poisson's ratio of fiber and matrix is the same, which implies the inexistence of transversal stress when the loading is applied along the fiber. Considering the displacements in the fiber u and distant from the fiber v: (Fig. 2.6):

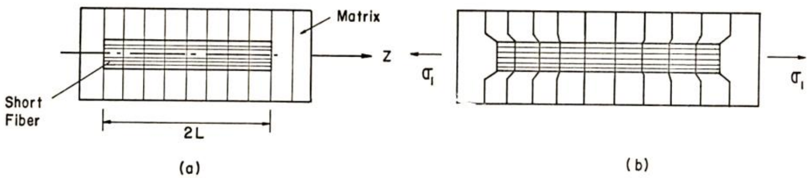

Fig. 2.6 Simplified scheme of the stress field around the fiber. a) without loading. b) loaded. [11]

From Hooke's Law and taking the differential:

$$\sigma = E\epsilon = \frac{P}{A} = E\,\frac{\ddot{o}}{L} \qquad \frac{dP}{dx} = \frac{EA}{L}\cdot\frac{d\ddot{o}}{dx} \tag{2.5}$$

Cox proposes similar behavior [31]:

$$\frac{dP_f}{dx} = B(u - v) \tag{2.6}$$

where P_f is the load acting on the fiber and B is a constant that depends on the fiber distribution and the Young's modulus of fiber and matrix.

Differentiation of Eq. 2.7 leads to:

$$\frac{d^2P_f}{dx^2} = B\left(\frac{du}{dx} - \frac{dv}{dx}\right) \tag{2.7}$$

The derivatives of u and v can be taken as the deformations in the fiber and matrix, respectively:

$$\frac{du}{dx} = \frac{P_f}{A_f E_f} \tag{2.8}$$

$$\frac{dv}{dx} = \varepsilon \tag{2.9}$$

Substitution of (2.8) and (2.9) in (2.7), gives:

$$\frac{d^2P_f}{dx^2} = B\left(\frac{P_f}{A_fE_f} - \varepsilon\right) \tag{2.10}$$

A solution to this differential equation leads to:

$$P_f = E_fA_f\varepsilon + Ssinh(\beta x) + Tcosh(\beta x) \tag{2.11}$$

where:

$$\beta = \sqrt{\frac{B}{E_fA_f}} \tag{2.12}$$

and S and T are constants depending on the boundary conditions of the system.

2.2.3 Strength statistics for fiber bundles

It is well-known for bundles of fibers, that the bundle strength is always less than the sum of the fiber strengths, sometimes as much as 50% [32-37]. This is because the fibers are real materials and thus they have variable properties, and so the statistical variation needs to be taken into effect, and also the grouping and overloading effect due to the grouping. In Fig. 2.7 typical Weibull plots for single fiber strength, the strength of a bundle of these fibers, and the strength of a composite made with the bundle are shown.

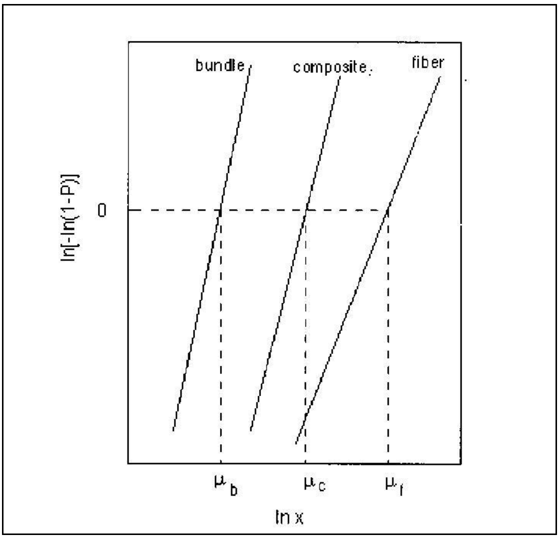

Fig. 2.7 Weibull plots for fiber tensile strength, bundle strength, and composite bundle strength [32].

Note that going from the fiber to the bundle, the average strength is decreased, but, as the bundle is made into a composite, the strength goes up; also notice that the Weibull modulus (m) increases, meaning the variability decreases. There are clearly things happening in the bundle and composite that cannot be explained deterministically.

2.2.3.1 Statistics for bundle strength. Daniel's Theorem

Consider a simple tensile experiment on a bundle of six fibers. Suppose that they are all the same size, and we know their breaking loads P_1 = 2.0 N, P_2 = 2.2 N, P_3 = 3.2 N, P_4 = 3.4 N, P_5 = 3.6 N and P_6 = 3.8 N. Assume that the bundle load when the load in each surviving fiber is P, $G_6(P)$ and denote the bundle strength by $G_6^*(P)$. In a deterministic world, an ultimate bundle strength $G_6^*(P)$ = 3.03, the average fiber strength, would be the value used [32].

Then, by putting the bundle of 6 fibers in a commercial testing machine and monotonically increasing the strain, a result as the Figure 2.8 is obtained. The load in each of the fibers is identical and increases until each fiber carries a load of 2 N, and then fiber #1 fails. The surviving fibers still carry a 2 N load, but now the bundle strength is only 0.83 of its original value at the instant that the fiber broke. Now continue the extension until #2 breaks at a fiber load of 2.2 N, and the bundle strength drops again [32].

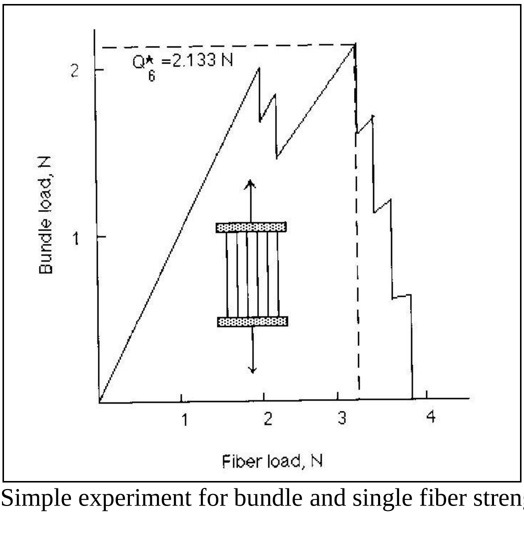

Fig. 2.8 Simple experiment for bundle and single fiber strength [32].

Continuing on until the remaining fibers break, the peak load in found to occur when fiber #3 breaks, and this is the bundle strength G*. A general expression for the bundle strength of a bundle with *n* fibers can be written [33]:

$$G_n^* = \max_{1 \le i \le n} \left\{ P_1, \frac{n-1}{n} P_2, ..., \frac{n-i+1}{n} P_i, ..., \frac{1}{n} P_n \right\} \qquad (2.13)$$

More desirable, however, is being able to predict the bundle strength distribution from a knowledge of the fiber strength distribution, as well as being able to predict the strength of a large bundle of fibers; as n reaches infinity, the calculation of the former expression becomes extremely tedious. Looking more closely at equation (2.13) it can be seen that the first of the two terms is the fraction of surviving fibers while the second is the load at which they are still surviving. Motivated by this, if F(σ) is the failure probability for the individual fibers in the bundle, then the bundle strength, G*(x) can be found to be [32]:

$$G^* = \{ \sup x \ge 0 | x \cdot [1 - F(\sigma)] \} \qquad (2.14)$$

Daniels [34] was the first one to provide an analytical result to predict the bundle strength (eq. 2.15). However, it can be seen that with an increasing number of fibers, the expression itself becomes really unfeasible to calculate.

$$G_n(x) = \sum_{i=1}^{n} (-1)^{i+1} \binom{n}{i} F(\sigma)^i G_{n-1}\left(\frac{n\sigma}{n-i} \right), x \ge 0 \qquad (2.15)$$

2.2.3.2 Load Sharing

In the model above it was assumed that, in a bundle under load, when a fiber fails, its load is shared equally among the surviving fibers. Such a load sharing arrangement is called an equal load sharing (ELS) rule [32-35]. Suppose the bundle load, G_n, on n fibers at the instant before the weakest fiber breaks is P-ε, where ε is very small. At this point each fiber carries the load. When the first fiber fails at P, under ELS, each of the remaining n-1 fibers must be overloaded to carry the load from the broken fiber, so each fiber immediately after the breakage will bear the load P(n/n-1). The term in brackets at eq. 2.16 is called the load concentration factor, in this case K_1. In general the ith load concentration factor, K_i, under ELS is [35]:

$$K_i = \left\lceil \frac{n}{n-i} \right\rceil, 1 \le i \le n-1 \qquad (2.16)$$

For example, suppose a bundle has 10 fibers and the weakest fiber has strength 1. When G_{10} = 1, the first fiber will break, and immediately, each fiber will now carry a load of 1.1. At this point there are a few possibilities depending upon the strength of the next weakest fiber. If the strength is higher or equal to 1.1, all of these fibers will survive to the failure of the first. But, if only one has strength lower than 1.1, it will fail immediately and the remaining fibers will bear a 1.25 load. That means, the failure of only one fiber can lead to the catastrophic failure of the bundle relating to the overloading of the remaining fibers [32,35].

This model has some interesting implications. First, it explains why the bundle strength is lower than the mean fiber strength, as seen on Fig. 3.11. Second, it shows that the way to increase the strength of the bundle is not by simply adding stronger fibers, but rather by removing the weak ones. Because of load transfer, when many weak fibers have failed the overload will be enough to overcome any contribution of the stronger fibers. Third, another way to increase the bundle strength is that the fiber strength distribution has a high mean and as little variability as possible [32,35].

2.2.3.3 Local Load Sharing

The equal load sharing rule generally gives the most conservative value for bundle strength. Moreover, because the matrix in a composite tends to isolate the effects of a fiber break to the immediate vicinity of the failed fiber, the fiber's immediate and nearest neighbors bear a larger part of the overload, more than a fiber at a some distance away. A number of alternate rules to ELS have been proposed, the simplest being local load sharing, LLS [33]. Under LLS the load carried by a broken fiber is transferred only to that fiber's nearest, unbroken neighbors. Figure 2.9 illustrates this rule for several arrangements of broken fibers within a 7-fiber bundle.

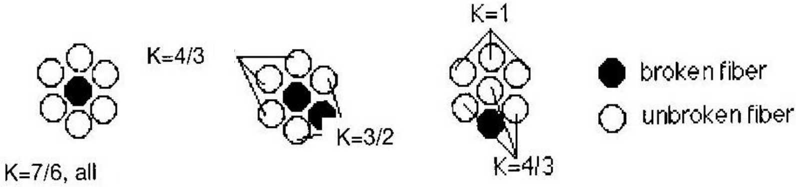

Fig. 2.9 Load intensity factors for a bundle of 7 fibers, assuming LLS [32].

Other important quantity is the number of fiber breaks required for the bundle to fail, called the critical cluster size, and is often denoted by k*. If we know the Weibull modulus for fiber strength, m, and find the Weibull modulus for bundle strength, β, then the critical cluster size is [32]:

$$k^* = \frac{\beta}{m} \tag{2.17}$$

When k* > 1, the Weibull modulus for bundle strength is higher than that for fiber strength, explaining the change in slope of the curves in Fig. 2.7.

3 MODELING

3.1 SIMPLIFIED SHEAR-LAG MODEL

3.1.1 Previous Considerations and Analysis

The majority of the load transfer models for short-fiber reinforced composites was created to describe the behavior of polymer matrix composites. These include the following assumptions:

- The elastic modulus of the fibers (E_f) is much higher than the matrix (E_m);
- The deformation until failure from the fibers (ε_f) is much lower than the matrix(ε_m);
- The matrix has some degree of ductility.

Those criteria are particularly not true in the case of ceramic matrix composites, where the material of the matrix is almost the same from the fibers, so it is possible to take into account different load sharing phenomena.

The proposed model in this Thesis tries to take into account the compatibility between the fibers and matrix in porous-matrix composites, by a function of load transfer in the tip of the fibers, inversely proportional to the porosity of the matrix. Some effort is made to approximate the load transfer functions, trying to avoid the use of hyperbolic functions, which will complicate further the solution of the problem.

3.1.2 Linear Shear-Lag Model

According to Fig. 3.1, let's consider a composite with fibers whose length is 2L, diameter 2r and Young's modulus E_f, embedded in a matrix with porosity ρ, made of the same material of the fiber. Hereby we define the critical length L_c, in which from the tip of the fiber the stress distribution isn't constant by the shear-lag between matrix and fiber. It is more feasible to work with α, the ratio between the critical length and fiber length, being $L_c = \alpha \cdot L$.

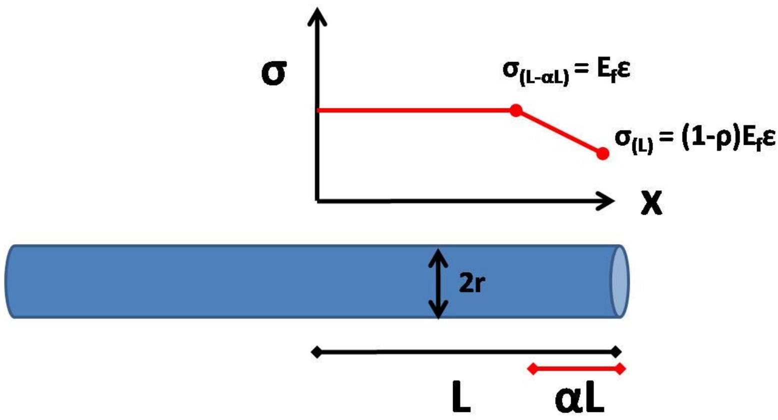

Fig. 3.1 Proposed stress distribution and boundary conditions

Therefore, it can be proposed that the stress distribution between the points L-αL and L follows a linear behavior such as:

$$\sigma_f(x) = Ax + B \tag{3.1}$$

By using the boundary conditions defined in Fig. 3.1, and substituting then in (3.1):

$$E_f\varepsilon = A(L - \alpha L) + B \tag{3.2}$$

$$(1-\rho)E_f\varepsilon = AL + B \tag{3.3}$$

Isolating B in (3.2) and replacing in (3.3):

$$(1-\rho)E_f\varepsilon - AL = E_f\varepsilon - A(L - \alpha L) \tag{3.4}$$

$$-\rho E_f\varepsilon = A\alpha L \tag{3.5}$$

And then:

$$A = -\frac{\rho E_f\varepsilon}{\alpha L} \tag{3.6}$$

By replacing A from (3.1) with (3.6):

$$(1-\rho)E_f\varepsilon = -\frac{\rho E_f\varepsilon}{\alpha} + B \tag{3.7}$$

Therefore, B is given by:

$$B = \left[1 - \rho\left(1 - \frac{1}{\alpha}\right)\right]E_f\varepsilon \tag{3.8}$$

By replacing the constants in (3.1), we have the stress distribution behavior:

$$\sigma_f(x) = -\frac{\rho E_f\varepsilon}{\alpha L}x + \left[1 - \rho\left(1 - \frac{1}{\alpha}\right)\right]E_f\varepsilon \tag{3.9}$$

To determine the shear stresses along the fiber, the force equilibrium in a fiber element with diameter 2r and length dx is made in the x direction, resulting in:

$$\partial\sigma \cdot \pi r^2 + \tau \cdot 2\pi r dx = 0 \tag{3.10}$$

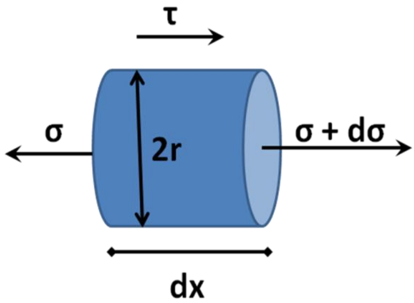

Fig. 3.2 Force equilibrium in an infinitesimal fiber element.

Then, the shear stresses are given by:

$$\tau = -\frac{r}{2}\frac{d\sigma}{dx} \tag{3.11}$$

By the differential of (3.9):

$$\tau_f(x) = \frac{r\rho E_f \varepsilon}{2\alpha L} \tag{3.12}$$

With the stress distribution along the fiber, it is possible to calculate the average stress carried by the fiber in the composite, given by:

$$\bar{\sigma_f} = \frac{1}{L}\int_0^L \sigma_f(x)\, dx \tag{3.13}$$

For α ≥ 1, i.e. the fiber is shorter than the critical length:

$$\bar{\sigma_f} = \frac{1}{L}\int_0^L -\frac{\rho E_f \varepsilon}{\alpha L}x + \left[1 - \rho\left(1 - \frac{1}{\alpha}\right)\right] E_f \varepsilon\, dx \tag{3.14}$$

Then,

$$\bar{\sigma_f} = \frac{-\frac{\rho E_f \varepsilon}{2\alpha L}L^2 + \left[1 - \rho\left(1 - \frac{1}{\alpha}\right)\right] E_f \varepsilon\, L}{L} \tag{3.15}$$

Simplifying the equation:

$$\bar{\sigma_f} = -\frac{\rho E_f \varepsilon}{2\alpha} + \left[1 - \rho\left(1 - \frac{1}{\alpha}\right)\right] E_f \varepsilon \tag{3.16}$$

$$\bar{\sigma_f} = \left[1 - \rho\left(1 - \frac{1}{\alpha}\right) - \frac{\rho}{2\alpha}\right] E_f \varepsilon \tag{3.17}$$

Therefore, the average stress carried by the fiber is given by:

$$\bar{\sigma_f} = \left[1 - \rho - \frac{\rho}{2\alpha}\right] E_f \varepsilon \tag{3.18}$$

And for $0 < \alpha < 1$, i.e., the fiber is longer than the critical length:

$$\bar{\sigma_f} = \frac{\int_0^{L-\alpha L} E_f \varepsilon \, dx + \int_{L-\alpha L}^{L} \sigma_f(x) \, dx}{L} \tag{3.19}$$

Then,

$$\bar{\sigma_f} = \frac{E_f \varepsilon (L - \alpha L) - \frac{\rho E_f \varepsilon}{\alpha L} \int_{L-\alpha L}^{L} x \, dx + \left[1 - \rho\left(1 - \frac{1}{\alpha}\right)\right] E_f \varepsilon \int_{L-\alpha L}^{L} dx}{L} \tag{3.20}$$

Therefore:

$$\bar{\sigma_f} = E_f \varepsilon (1 - \alpha) - \frac{\rho E_f \varepsilon}{\alpha}\left[\frac{1}{2} - \frac{(1-\alpha)^2}{2}\right] + \left[1 - \rho\left(1 - \frac{1}{\alpha}\right)\right] \alpha E_f \varepsilon \tag{3.21}$$

$$\bar{\sigma_f} = E_f \varepsilon (1 - \alpha) - \rho E_f \varepsilon \left[\frac{2 + \alpha}{2}\right] + \left[1 - \rho\left(1 - \frac{1}{\alpha}\right)\right] \alpha E_f \varepsilon \tag{3.22}$$

$$\bar{\sigma_f} = E_f \varepsilon \left(1 - \alpha - \rho + \frac{\rho\alpha}{2} + \alpha - \rho\alpha + \rho\right) \tag{3.23}$$

Simplifying the equations, we get the average stress carried by the fibers longer than the critical length:

$$\bar{\sigma_f} = E_f \varepsilon \left(1 - \frac{\rho\alpha}{2}\right) \tag{3.24}$$

With the average stresses well defined, we can define the stresses in the ply longitudinal and transversal directions. When the matrix material is the same as the fiber, it is possible to write the elastic modulus of the matrix in a function of the fiber modulus:

$$E_m = E_f e^{-bp} \tag{3.25}$$

where b is a shape factor that depends on the pore shape and distribution, according to Watchman [38].

The stress on the transversal direction is equal to the matrix maximum stress, given by:

$$\sigma_T = \sigma_m = E_f \varepsilon e^{-bp} \tag{3.26}$$

The stress on the longitudinal direction is given by the average value between matrix and fiber, based on the volumetric fractions of fiber and matrix:

$$\sigma_L = \sigma_m (1 - v_f) + \bar{\sigma_f} v_f = (1 - v_f) E_f \varepsilon e^{-bp} + \bar{\sigma_f} v_f \tag{3.27}$$

Therefore for $0 < \alpha < 1$:

$$\sigma_L = (1 - v_f) E_f \varepsilon e^{-bp} + E_f \varepsilon \left(1 - \frac{\rho\alpha}{2}\right) v_f \tag{3.28}$$

And for $\alpha > 1$:

$$\sigma_L = (1 - v_f) E_f \varepsilon e^{-bp} + E_f \varepsilon \left[1 - \rho - \frac{\rho}{2\alpha}\right] v_f \tag{3.29}$$

3.1.3 Quadratic Shear-Lag Model

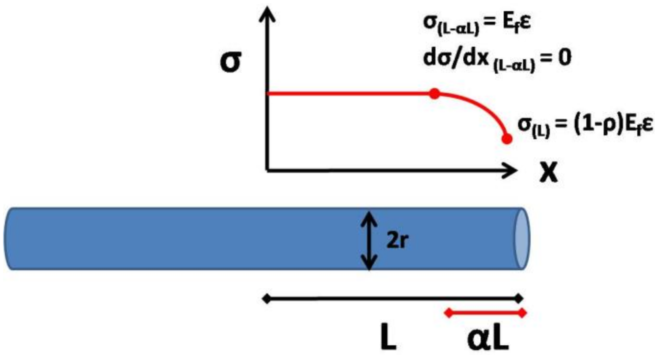

Fig. 3.3 Proposed stress distribution and boundary conditions

In a similar manner as the linear model, it can be proposed that the stress distribution between the points L-αL and L follows a quadratic behavior such as:

$$\sigma_f(x) = Ax^2 + Bx + C \tag{3.30}$$

By using the boundary conditions given in Fig. 3.3, and substituting then in (3.30):

$$E_f\varepsilon = A(L-\alpha L)^2 + B(L-\alpha L) + C \tag{3.31}$$

$$(1-\rho)E_f\varepsilon = AL^2 + BL + C \tag{3.32}$$

$$0 = 2A(L-\alpha L) + B \tag{3.33}$$

Isolating B in (3.33) and replacing in (3.31) and (3.32):

$$B = -2A(L-\alpha L) \tag{3.34}$$

$$E_f\varepsilon = A(L-\alpha L)^2 - 2A(L-\alpha L)^2 + C = -A(L-\alpha L)^2 + C \tag{3.35}$$

$$(1-\rho)E_f\varepsilon = AL^2 - 2AL(L-\alpha L) + C \tag{3.36}$$

Subtracting (3.36) from (3.35):

$$\rho E_f\varepsilon = -A(L-\alpha L)^2 - AL^2 + 2AL(L-\alpha L) \tag{3.37}$$

$$\rho E_f\varepsilon = -AL^2(1-2\alpha+\alpha^2) - AL^2 + 2AL^2 - 2\alpha AL^2 \tag{3.38}$$

$$\rho E_f\varepsilon = -AL^2(1-2\alpha+\alpha^2+1-2+2\alpha) \tag{3.39}$$

$$\rho E_f\varepsilon = -A\alpha^2L^2 \tag{3.40}$$

And then:

$$A = -\frac{\rho E_f\varepsilon}{\alpha^2L^2} \tag{3.41}$$

By replacing A from (3.33):

$$B = -2\left(-\frac{\rho E_f\varepsilon}{\alpha^2L^2}\right)(L-\alpha L) \tag{3.42}$$

Therefore, B is given by:

$$B = 2\frac{\rho E_f \varepsilon}{\alpha^2 L}(1-\alpha) \tag{3.43}$$

To find C, we replace A in (3.34):

$$E_f \varepsilon = \frac{\rho E_f \varepsilon}{\alpha^2 L^2}(L-\alpha L)^2 + C \tag{3.44}$$

$$C = E_f \varepsilon - \frac{\rho E_f \varepsilon}{\alpha^2}(1-\alpha)^2 \tag{3.45}$$

By replacing the constants in (3.30), we have the stress distribution behavior:

$$\sigma_f(x) = -\frac{\rho E_f \varepsilon}{\alpha^2 L^2}\,x^2 + 2\frac{\rho E_f \varepsilon}{\alpha^2 L}(1-\alpha)\,x + E_f \varepsilon - \frac{\rho E_f \varepsilon}{\alpha^2}(1-\alpha)^2 \tag{3.46}$$

To determine the shear stresses along the fiber, the force equilibrium in a fiber element with diameter 2r and length dx is made in the x direction, resulting in:

$$\partial\sigma \cdot \pi r^2 + \tau \cdot 2\pi r dx = 0 \tag{3.10}$$

Then, the shear stresses are given by:

$$\tau = -\frac{r}{2}\frac{d\sigma}{dx} \tag{3.11}$$

By the differential of (3.46):

$$\tau_f(x) = \frac{r\rho E_f \varepsilon}{\alpha^2 L}\left[\frac{1}{L}\,x - 1 + \alpha\right] \tag{3.47}$$

With the stress distribution along the fiber, it is possible to calculate the average stress carried by the fiber in the composite, given by:

$$\bar{\sigma_f} = \frac{1}{L}\int_0^L \sigma_f(x)\,dx \tag{3.13}$$

For $\alpha \geq 1$, i.e. the fiber is shorter than the critical length:

$$\bar{\sigma_f} = \frac{1}{L}\int_0^L \left[-\frac{\rho E_f \varepsilon}{\alpha^2 L^2}\,x^2 + 2\frac{\rho E_f \varepsilon}{\alpha^2 L}(1-\alpha)\,x + E_f \varepsilon - \frac{\rho E_f \varepsilon}{\alpha^2}(1-\alpha)^2\right]dx \tag{3.48}$$

Then,

$$\bar{\sigma_f} = \frac{-\frac{\rho E_f \varepsilon}{3\alpha^2 L^2}\,L^3 + \frac{\rho E_f \varepsilon}{\alpha^2 L}(1-\alpha)\,L^2 + E_f \varepsilon\,L - \frac{\rho E_f \varepsilon}{\alpha^2}(1-\alpha)^2 L}{L} \tag{3.49}$$

Simplifying the equation:

$$\bar{\sigma_f} = -\frac{\rho E_f \varepsilon}{3\alpha^2} + \frac{\rho E_f \varepsilon}{\alpha^2}(1-\alpha) + E_f \varepsilon - \frac{\rho E_f \varepsilon}{\alpha^2}(1-\alpha)^2 \tag{3.50}$$

$$\bar{\sigma_f} = \left[1 + \frac{\rho}{\alpha^2}\left(\frac{2}{3}-\alpha\right) - \frac{\rho}{\alpha^2}(1-\alpha)^2\right]E_f \varepsilon \tag{3.51}$$

$$\bar{\sigma_f} = \left[1 + \frac{\rho}{\alpha^2}\left(\frac{2}{3}-\alpha-1+2\alpha-\alpha^2\right)\right]E_f \varepsilon \tag{3.52}$$

Therefore, the average stress carried by the fiber is given by:

$$\bar{\sigma_f} = \left[1 - \rho\left(\frac{1}{3\alpha^2} - \frac{1}{\alpha} + 1\right)\right] E_f \varepsilon \tag{3.53}$$

And for $0 < \alpha < 1$, i.e., the fiber is longer than the critical length:

$$\bar{\sigma_f} = \frac{\int_0^{L-\alpha L} E_f \varepsilon \, dx + \int_{L-\alpha L}^{L} \sigma_f(x)\, dx}{L} \tag{3.54}$$

Therefore:

$$\begin{aligned}\bar{\sigma_f} = E_f \varepsilon(1-\alpha) - \frac{\rho E_f \varepsilon}{\alpha^2}\left[\frac{1}{3} - \frac{(1-\alpha)^3}{3}\right] + 2\frac{\rho E_f \varepsilon}{\alpha^2}(1-\alpha)\left[\frac{1}{2} - \frac{(1-\alpha)^2}{2}\right] \\ + \left[E_f \varepsilon - \frac{\rho E_f \varepsilon}{\alpha^2}(1-\alpha)^2\right](1-1+\alpha)\end{aligned} \tag{3.55}$$

$$\begin{aligned}\frac{\bar{\sigma_f}}{E_f \varepsilon} = 1 - \alpha - \frac{\rho}{\alpha^2}\left[\frac{1}{3} - \frac{(1-\alpha)^3}{3}\right] + 2\frac{\rho}{\alpha^2}(1-\alpha)\left[\frac{1}{2} - \frac{(1-\alpha)^2}{2}\right] \\ + \left[1 - \frac{\rho}{\alpha^2}(1-\alpha)^2\right](1-1+\alpha)\end{aligned} \tag{3.56}$$

$$\begin{aligned}\frac{\bar{\sigma_f}}{E_f \varepsilon} = 1 - \alpha - \left[\frac{\rho}{3\alpha^2} - \frac{\rho(1-\alpha)^3}{3\alpha^2}\right] + 2\frac{\rho}{\alpha^2}\left[\frac{1}{2} - \frac{(1-\alpha)^2}{2} - \frac{\alpha}{2} + \frac{\alpha(1-\alpha)^2}{2}\right] \\ + \left[\alpha - \frac{\rho}{\alpha}(1-\alpha)^2\right]\end{aligned} \tag{3.57}$$

$$\begin{aligned}\frac{\bar{\sigma_f}}{E_f \varepsilon} = 1 - \frac{\rho}{3\alpha^2}[1 - 1 + 3\alpha - 3\alpha^2 + \alpha^3] \\ + \frac{\rho}{\alpha^2}[1 - 1 + 2\alpha - \alpha^2 - \alpha + \alpha - 2\alpha^2 + \alpha^3] - \frac{\rho}{\alpha}(1-\alpha)^2\end{aligned} \tag{3.58}$$

$$\frac{\bar{\sigma_f}}{E_f \varepsilon} = 1 - \frac{\rho}{\alpha}\left[1 - \alpha + \frac{\alpha^2}{3}\right] + \frac{\rho}{\alpha}[2 - 3\alpha + \alpha^2] - \frac{\rho}{\alpha}(1-\alpha)^2 \tag{3.59}$$

$$\frac{\bar{\sigma_f}}{E_f \varepsilon} = 1 - \frac{\rho}{\alpha}\left[1 - \alpha + \frac{\alpha^2}{3} - 2 + 3\alpha - \alpha^2 + 1 - 2\alpha + \alpha^2\right] \tag{3.60}$$

Simplifying the equations, we get the average stress carried by the fibers longer than the critical length:

$$\bar{\sigma_f} = E_f \varepsilon\left(1 - \frac{\rho\alpha}{3}\right) \tag{3.61}$$

With the average stresses well defined, we can define the stresses in the ply longitudinal and transversal directions. When the matrix material is the same as the fiber, it is possible to write the elastic modulus of the matrix in a function of the fiber modulus:

$$E_m = E_f e^{-bp} \tag{3.25}$$

where b is a shape factor that depends on the pore shape and distribution, as discussed previously.

The stress on the transversal direction is equal to the matrix maximum stress, given by:

$$\sigma_T = \sigma_m = E_f \varepsilon e^{-bp} \tag{3.26}$$

The stress on the longitudinal direction is given by the average value between matrix and fiber, based on the volumetric fractions of fiber and matrix:

$$\sigma_L = \sigma_m(1 - v_f) + \bar{\sigma}_f v_f = (1 - v_f)E_f \varepsilon e^{-bp} + \bar{\sigma}_f v_f \tag{3.27}$$

Therefore for $0 < \alpha < 1$:

$$\sigma_L = (1 - v_f)E_f \varepsilon e^{-bp} + E_f \varepsilon \left(1 - \frac{\rho\alpha}{3}\right) v_f \tag{3.62}$$

And for $\alpha > 1$:

$$\sigma_L = (1 - v_f)E_f \varepsilon e^{-bp} + E_f \varepsilon \left[1 - \rho\left(\frac{1}{3\alpha^2} - \frac{1}{\alpha} + 1\right)\right] v_f \tag{3.63}$$

3.2 MONTE CARLO SIMULATION OF BUNDLE TESTING

The approach used to predict the ceramic bundle strength was a Monte-Carlo simulation of a tensile bundle test of dry fibers. The Matlab algorithm consisted of two main steps: generation of a random fiber bundle based on the Weibull parameters of single-fiber testing (Fig. 3.4) and simulated test of the created bundle (Fig. 3.5).

A Matlab routine was created in order to simulate the mechanical behavior of fiber bundles, with different load sharing rules, as a way to take into account the effects of processing and matrix in the fiber bundles.

The main steps on the simulation are the following:

- Generation of bundle of n fibers via a random fiber population from input Weibull parameters (m and σ_0);
- Increasing the load stepwise and individually compares it with the fibers. If the load is not enough to break a fiber, the load is increased. Otherwise, the compared fiber is broken and the load is redistributed according to the load-sharing rule;
- The above step is repeated until all fibers are broken;
- The ultimate load is recorded and the whole procedure is repeated 50 times in order to obtain a Weibull distribution;
- The program calculates the output Weibull parameters in bundle testing.

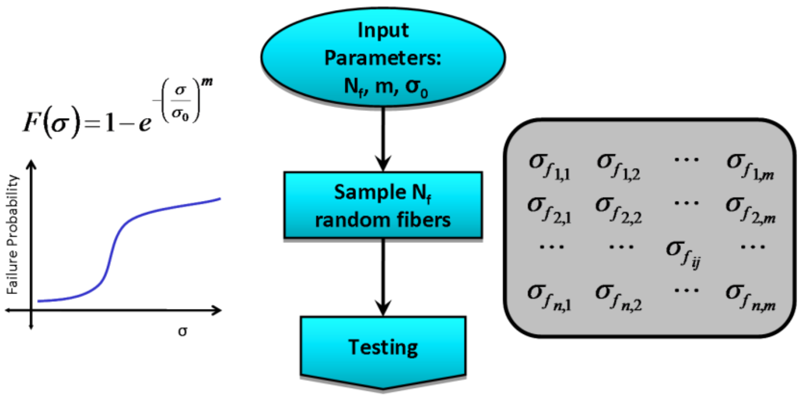

Fig 3.4 Scheme of the bundle generation algortithm.

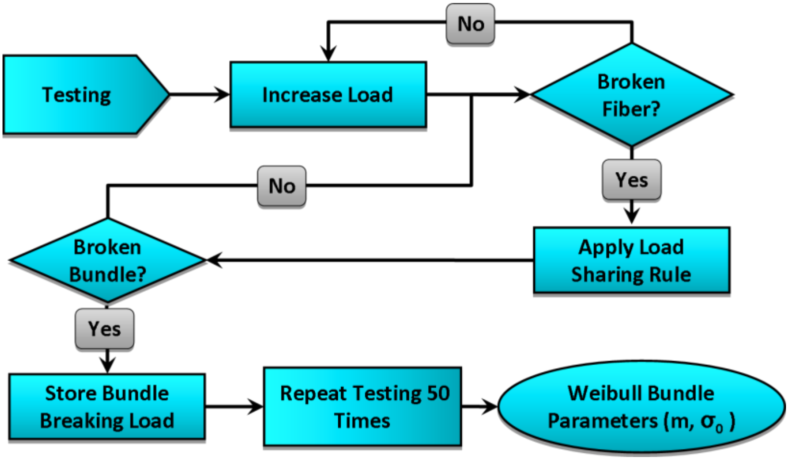

Fig 3.5 Scheme of the bundle testing algorithm.

3.2.1 Implementation of Load Sharing

The basis for the implementation of the load sharing is in the concept of load concentration factor, K. The bundle is seen by the program as a matrix of N×M fibers, each with a random breaking load, based on the Weibull distribution of the single fiber data.

The program compares this bundle-matrix with the load in the machine, if one fiber breaks, this load is multiplied by a load concentration matrix, K, which has also N×M items. In the case of equal load sharing, this factor is simply the total of fibers in the bundle divided by the number of remaining fibers.

In the case of local load sharing, whenever a fiber fails, it is marked and the program counts for each fiber the number of fractured neighbors, as can be seen in Fig. 3.6 for a hexagonal array. The failed fibers are the red Xs.

```
0   1   1   0   0   0   0   0
  1   X   1   0   0   0   0   0
0   1   1   0   0   0   0   0
  1   1   0   0   1   2   1   0
1   X   1   0   1   X   X   1
  1   1   0   0   1   2   1   0
0   0   0   0   0   0   0   0
```

Fig 3.6 Neighbor counting in a hexagonal array.

Then, the load concentration factor is calculated from the literature, based on the number of failed neighbors, according to Table 3.1.

Table 3.1 Load concentration factors

Number of Broken Neighbors	Circular LLS Rule	Argon, Elastic Matrix	Zweben and Rosen
0	1	1	1
1	1.5	1.49	1.33
2	2	1.76	1.6
3	2.5	1.92	1.83
4	3	2.07	2.03
10	6	2.72	2.97

Also, the neighbor counting method can be done in two ways: Considering a square (Fig. 3.7) or a hexagonal (Fig. 3.8) array. The implementation of the hexagonal array on a matrix is also shown, just being implemented by conditional counting in odd or even rows.

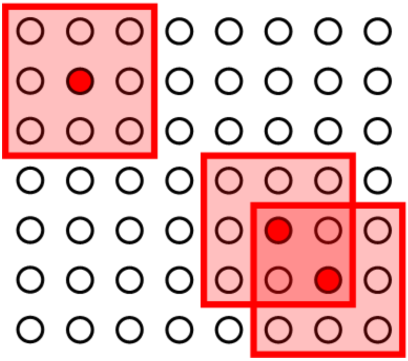

Fig 3.7 Neighbor counting for a square array.

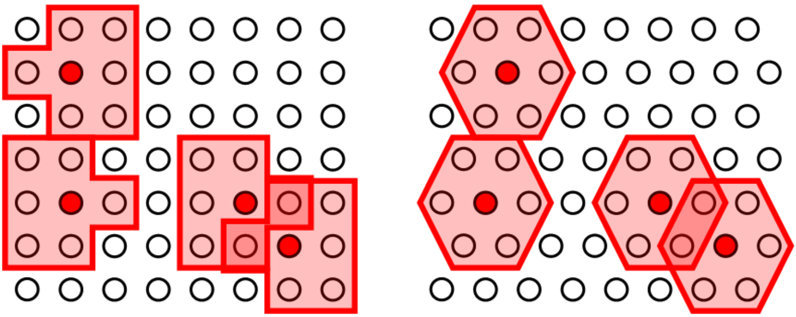

Fig 3.8 Neighbor counting for a hexagonal array.

4 MATERIALS AND METHODS

4.1 FIBER PREPARATION AND SAMPLE MOUNT DESIGN

Textiles of Nextel 610 fibers were obtained from 3M for the purposes of this study. The fiber bundles were carefully separated from the textiles and the fibers were desized according to the manufacturer's recommendations. The Nextel fibers could not be easily placed into the testing grips, due to their small size and fragile nature. Through multiple trials, key aspects that came to light regarding the testing of individual fibers included fiber handling, successfully loading fibers for testing, and preserving fibers so that fracture surfaces of the tested fibers could be examined. As a result, a sample mount technique was adapted from techniques available on the literature and modified to fit with this examination [39].

Providing support for handling of the Nextel fibers, while still allowing for the ease of tensile testing, was of main importance. Index cards were cut to 70 mm in length and 50 mm in width, with a hole with a diameter of 25mm punched in the center (Fig. 4.1). A fiber would then be glued into place on the card using superglue (cyanoacrylate glue). Once secured in the tensile grips, the card was then separated into two separate pieces through the use of a scissor. The same approach was used to the tensile testing of bundles, although the literature [40] recommends different gripping methods, in order to produce comparable results between single-fiber and bundle testing.

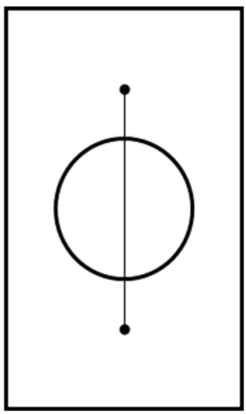

Fig. 4.1 Single fiber specimen mounted on the clamps for testing.

4.2 TENSILE TESTING

The tensile testing of single fibers and bundles (1500 den, ~400 fibers per bundle) was conducted with a controlled load on a Instron testing machine, with a 5N and 200 kN (for single-fiber and bundle tests, respectively) load cell using fiber tension test clamps. The fibers were tested using a controlled deformation mode, with preloading and a constant displacement ramp rate of 1 mm/min to a maximum of 4000 MPa. At least 29 specimens were tested in order to determine the statistical distribution.

4.3 DATA TREATMENT

In order to observe the statistical nature of the fiber and bundle strength, the resulting values on the mechanical testing were plotted according to Weibull's distribution (4.1).

$$P_f = 1 - e^{-\left(\frac{\sigma}{\sigma_0}\right)^m} \tag{4.1}$$

The mechanical testing data was ranked and each one was given a failure probability of n/N+1, were n is the rank of the data and N is the total number of tests. Those values were fitted with the linearized form of the distribution (4.2), yielding to the m and σ_0 values of the distribution (Fig. 4.2).

$$\ln\left(-\ln\left(1-P_f\right)\right) = m\ln\sigma - m\ln\sigma_0 \tag{4.1}$$

Table 4.1 Data Treatment for the fiber testing.

Data Rank	***Pf***	***Load (N)***	***ln(-ln(1-Pf))***	***Tensile Strength (MPa)***	***ln(σ)***
1	0,033	47,3	-3,384	1215,9	7,103
2	0,067	49,2	-2,697	1264,7	7,142
3	0,1	49,3	-2,250	1267,3	7,144
4	0,133	52,6	-1,944	1352,1	7,209
5	0,166	54,9	-1,701	1411,3	7,252
...	...	...	...	...	...

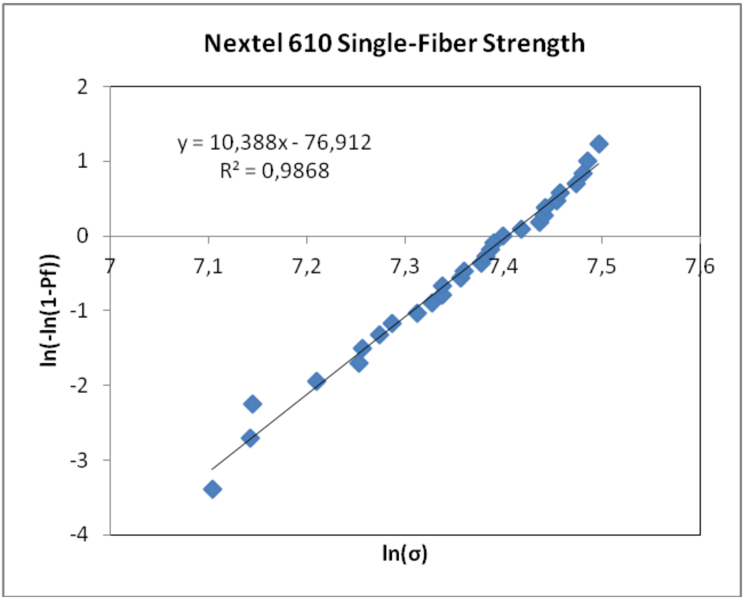

Fig. 4.2 Weibull fit of the single-fiber testing.

5 RESULTS AND DISCUSSION

5.1 SHEAR-LAG MODEL THEORETICAL RESULTS

To evaluate the models herein described, it is possible to apply the equations to an idealized composite, made of a porous alumina matrix and alumina fibers. The following table summarizes the important properties, taken as typical values from the literature:

Table 5.1 Simulated Composite Properties.

Property	Value
Fiber Volume Fraction	0.45
Matrix Porosity (%)	24
Fiber Length – 2L (mm)	50.8
Fiber Diameter (µm)	10
Critical Length / Length Ratio (α)	0.25

5.1.1 Linear Shear-Lag Model

5.1.1.1 Stress distribution

$$\sigma_f(x) = -\frac{\rho E_f \varepsilon}{\alpha L} x + \left[1 - \rho\left(1 - \frac{1}{\alpha}\right)\right] E_f \varepsilon \qquad (3.9)$$

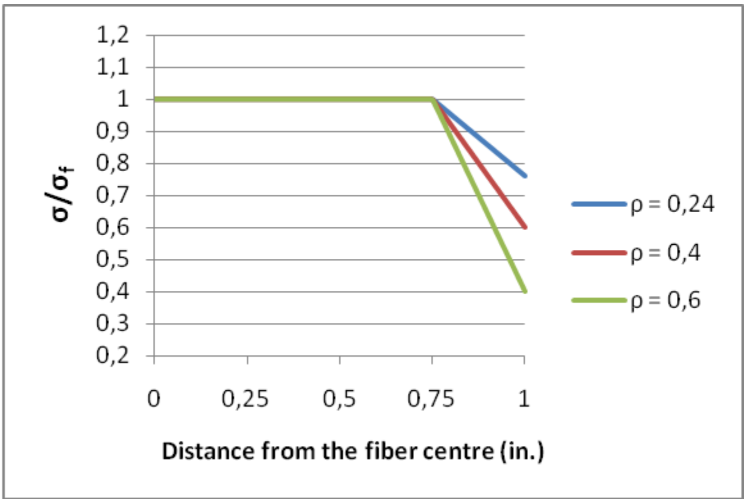

Fig. 5.1 Stress distribution along the fiber, for different matrix porosities.

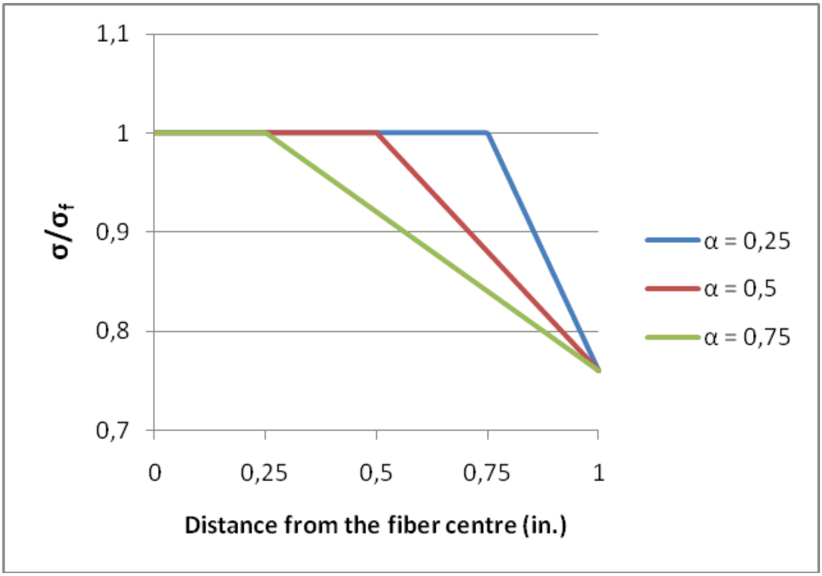

Fig. 5.2 Stress distribution along the fiber, for critical length ratios.

5.1.1.2 Shear Stresses

$$\tau_f(x) = \frac{r\rho E_f \varepsilon}{2\alpha L} \tag{3.12}$$

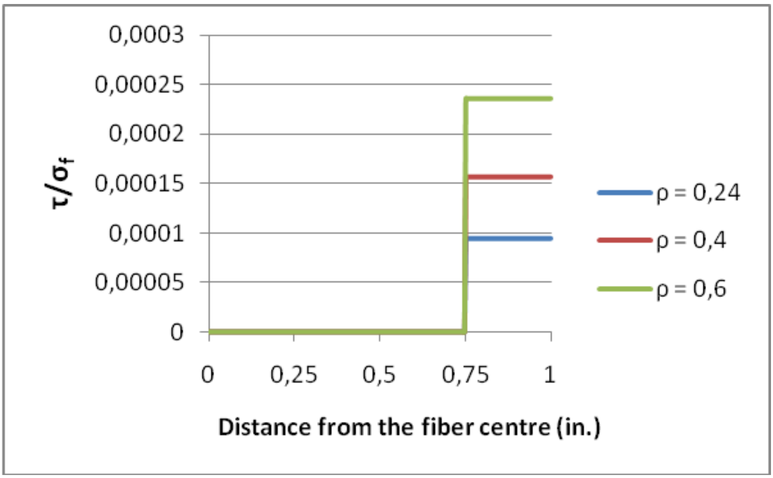

Fig. 5.3 Shear stress distribution along the fiber, for different matrix porosities.

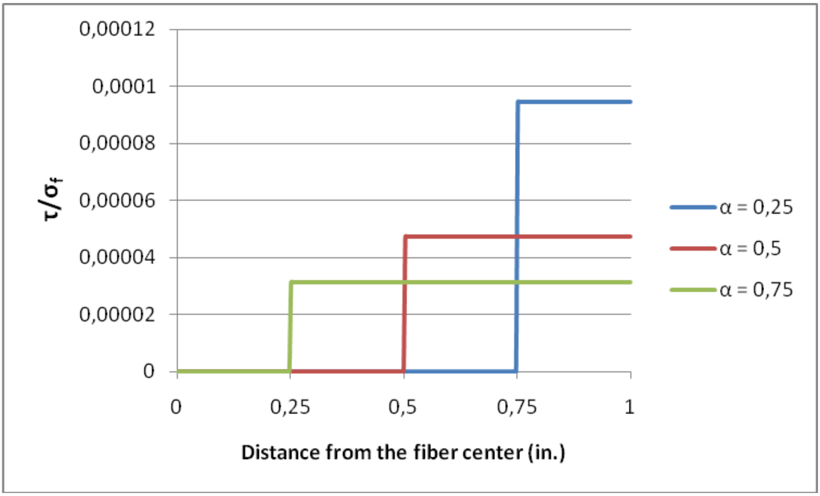

Fig. 5.4 Shear stress distribution along the fiber, for critical length ratios.

5.1.1.3 Average Stresses

$$\bar{\sigma_f} = \left[1 - \rho - \frac{\rho}{2\alpha}\right] E_f\, \varepsilon \qquad \text{for } \alpha > 1 \qquad (3.18)$$

$$\bar{\sigma_f} = E_f\, \varepsilon \left(1 - \frac{\rho\alpha}{2}\right) \qquad \text{for } 1 \geq \alpha \geq 0 \qquad (3.24)$$

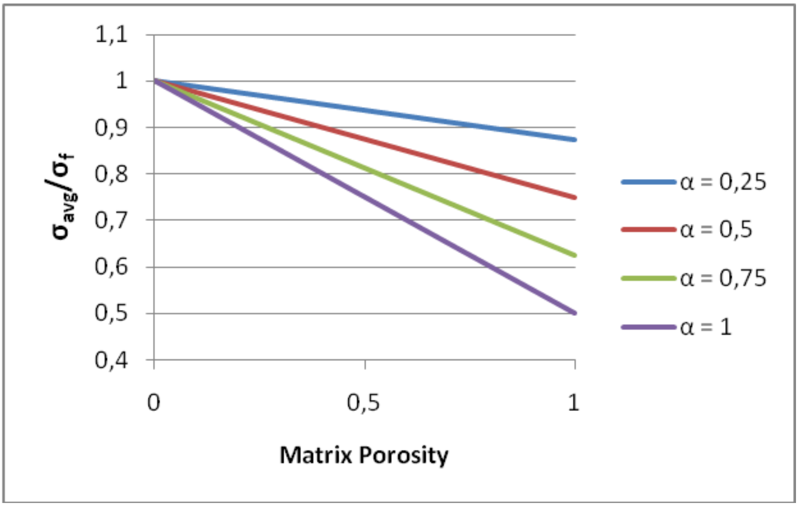

Fig. 5.5 Average stress carried by the fiber, for critical length ratios.

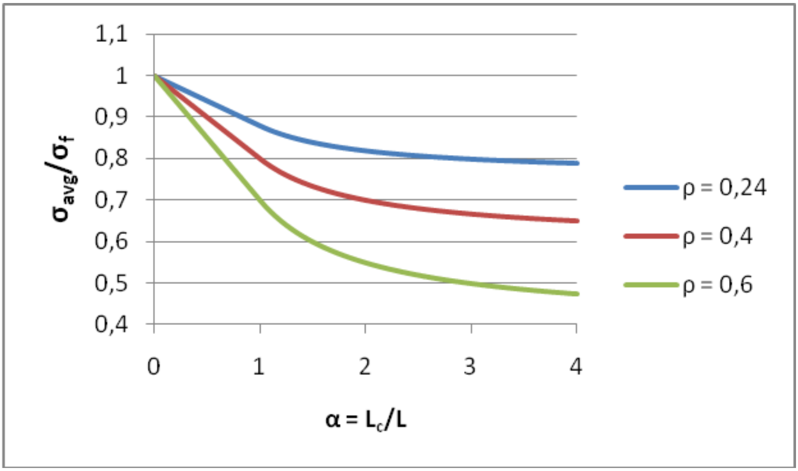

Fig. 5.6 Average stress carried by the fiber, for different matrix porosities.

5.1.1.4 Longitudinal Ply Strength

$$\sigma_L = (1 - v_f)E_f \varepsilon e^{-bp} + E_f \varepsilon \left(1 - \frac{\rho\alpha}{2}\right) v_f \qquad \text{for } 0 < \alpha < 1 \qquad (3.28)$$

$$\sigma_L = (1 - v_f)E_f \varepsilon e^{-bp} + E_f \varepsilon \left[1 - \rho - \frac{\rho}{2\alpha}\right] v_f \qquad \text{for } \alpha > 1 \qquad (3.29)$$

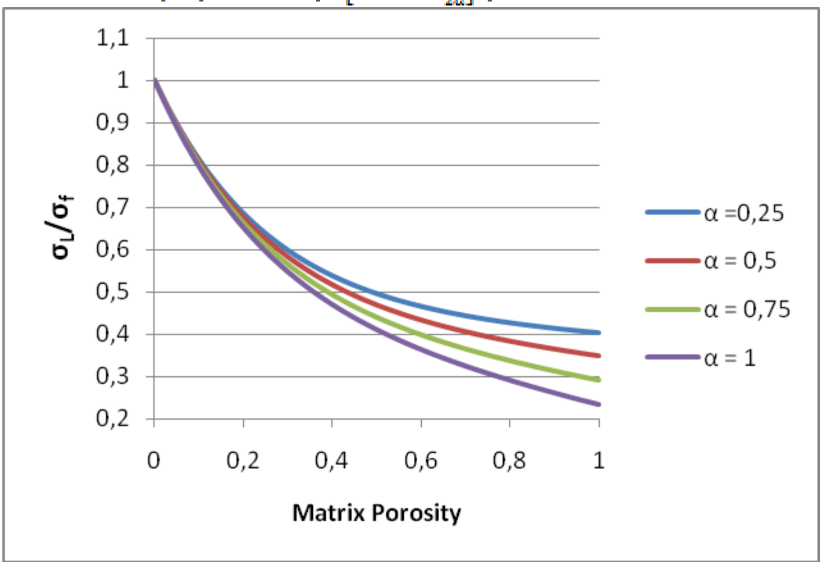

Fig. 5.7 Longitudinal Ply Strength, for critical length ratios.

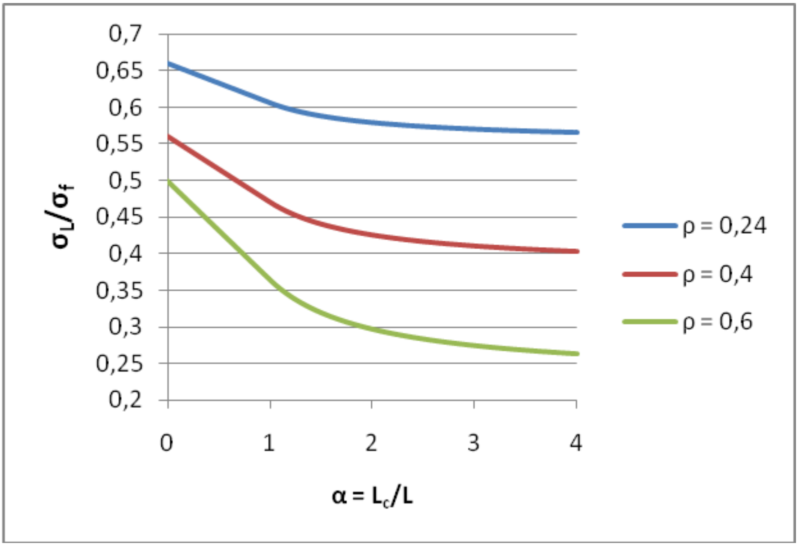

Fig. 5.8 Longitudinal Ply Strength, for different matrix porosities.

5.1.2 Quadratic Shear-Lag Model

5.1.2.1 Stress distribution

$$\sigma_f(x) = -\frac{\rho E_f \varepsilon}{\alpha^2 L^2}\, x^2 + 2\,\frac{\rho E_f \varepsilon}{\alpha^2 L}(1-\alpha)\, x + E_f\, \varepsilon - \frac{\rho E_f\, \varepsilon}{\alpha^2}(1-\alpha)^2 \qquad (3.46)$$

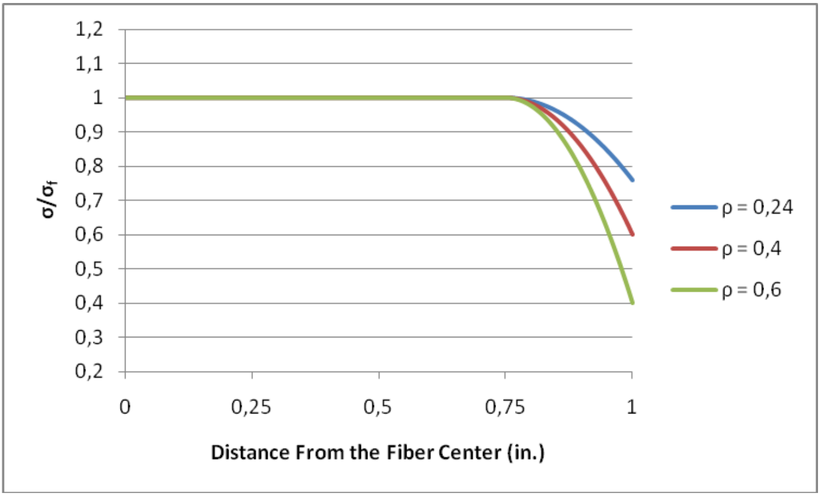

Fig. 5.9 Stress distribution along the fiber, for different matrix porosities.

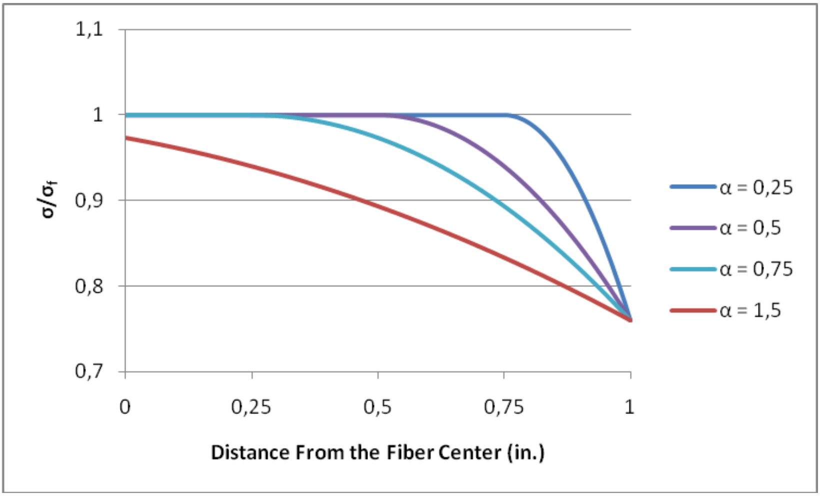

Fig. 5.10 Stress distribution along the fiber, for critical length ratios.

5.1.2.2 Shear Stresses

$$\tau_f(x) = \frac{r\rho E_f \varepsilon}{\alpha^2 L}\left[\frac{1}{L}\,x - 1 + \alpha\right] \qquad (3.47)$$

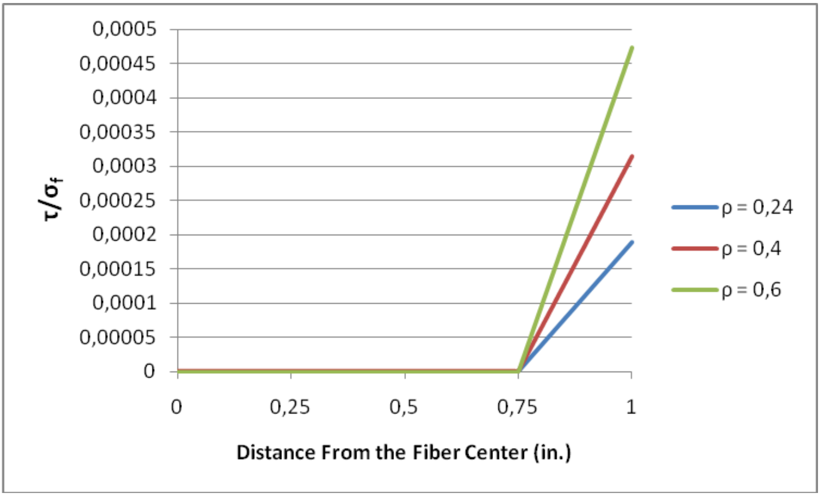

Fig. 5.11 Shear stress distribution along the fiber, for different matrix porosities.

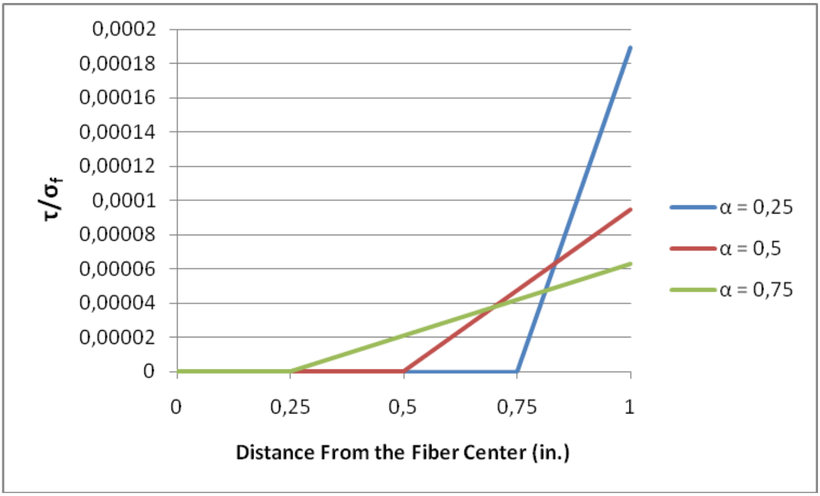

Fig. 5.12 Shear stress distribution along the fiber, for critical length ratios.

5.1.2.3 Average Stresses

$$\bar{\sigma_f} = \left[1 - \rho\left(\frac{1}{3\alpha^2} - \frac{1}{\alpha} + 1\right)\right] E_f \varepsilon \qquad \text{for } \alpha > 1 \qquad (3.53)$$

$$\bar{\sigma_f} = E_f \varepsilon \left(1 - \frac{\rho\alpha}{3}\right) \qquad \text{for } 1 \geq \alpha \geq 0 \qquad (3.61)$$

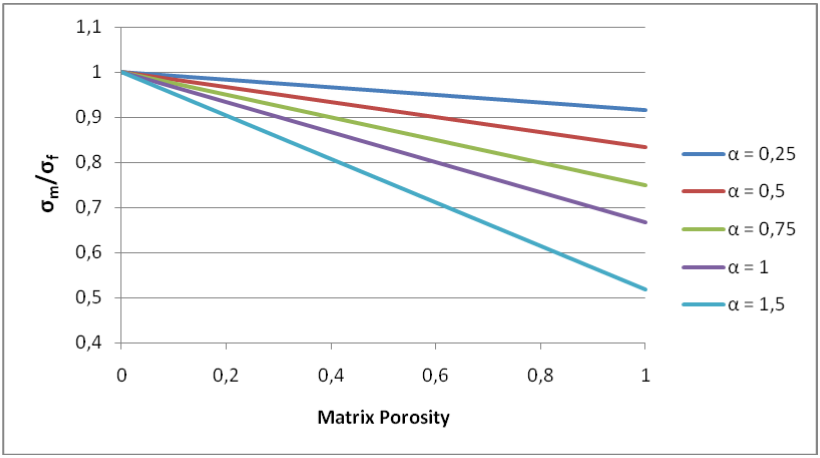

Fig. 5.13 Average stress carried by the fiber, for critical length ratios.

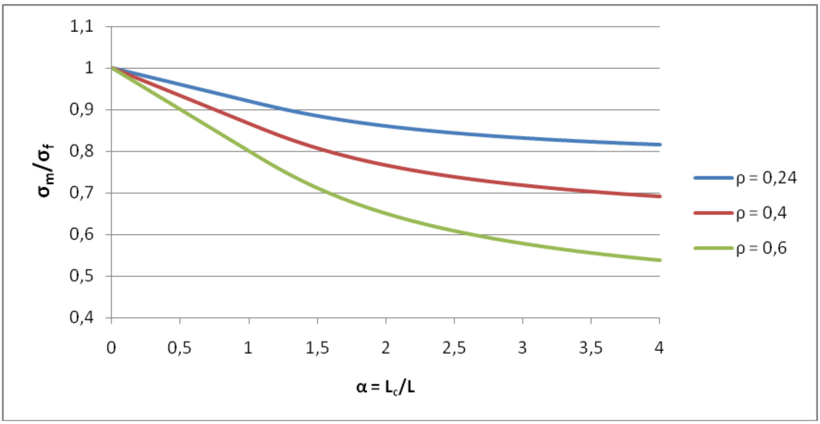

Fig. 5.14 Average stress carried by the fiber, for different matrix porosities

5.1.2.4 Longitudinal Ply Strength

$$\sigma_L = (1 - v_f)E_f\varepsilon e^{-bp} + E_f\varepsilon\left(1 - \frac{\rho\alpha}{3}\right)v_f \quad \text{for } 0 < \alpha < 1 \qquad (3.62)$$

$$\sigma_L = (1 - v_f)E_f\varepsilon e^{-bp} + E_f\varepsilon\left[1 - \rho\left(\frac{1}{3\alpha^2} - \frac{1}{\alpha} + 1\right)\right]v_f \quad \text{for } \alpha > 1 \qquad (3.63)$$

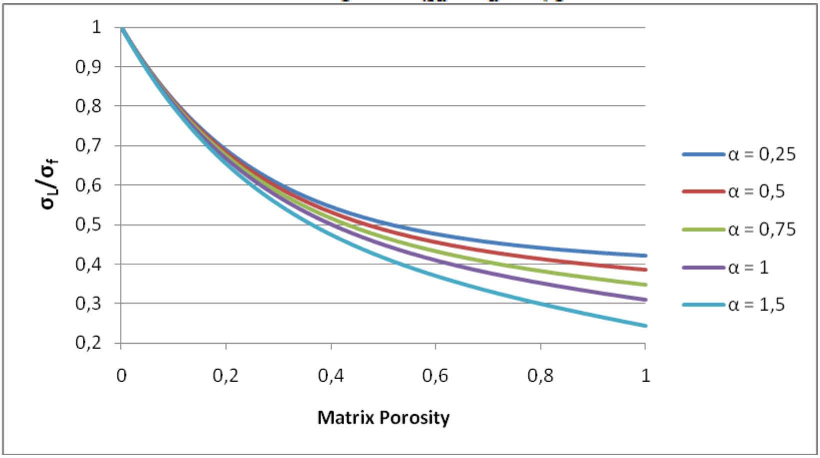

Fig. 5.15 Longitudinal Ply Strength, for critical length ratios.

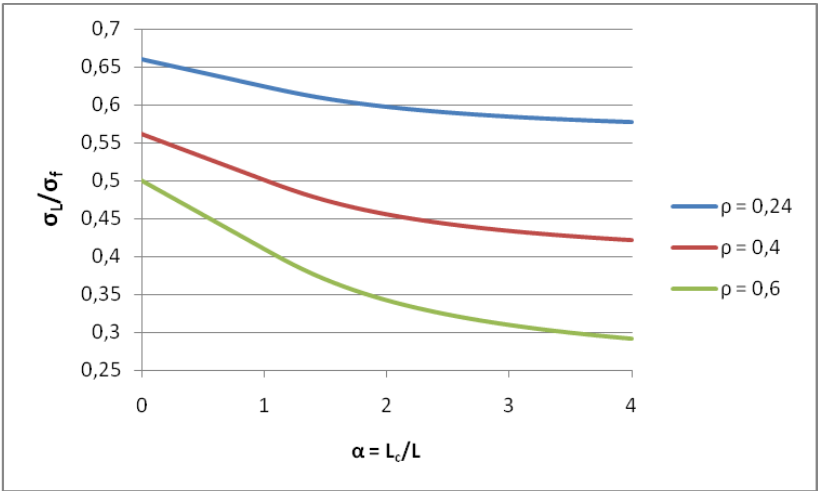

Fig. 5.16 Longitudinal Ply Strength, for different matrix porosities.

5.1.3 Comparison with Literature

As to evaluate the effectiveness of the models developed, model predictions are compared to a porous silicon carbide matrix composite reinforced with random-aligned silicon carbide fibers, as reported by Qin et al. [41].

The following parameters are assumed in order to make the calculations:

Table 5.2 Simulated Composite Properties.

Property	Value
Fiber Volume Fraction [41]	0.53
Fiber Length – 2L (mm) [41]	0.3-1
Fiber Diameter (μm) [41]	13
Bulk bending strength (MPa) [41]	300
Critical Length / Length Ratio, α	1
Fiber and bulk density (g/cm³) [41]	2.5
Sintering parameter, b [38]	4

The matrix porosity was obtained from the published composite densities, using the law of mixtures [11], leading to the following equation:

$$p_m = 1 - \frac{\rho_c - v_f \rho_f}{\rho_{th}\left(1 - v_f\right)} \tag{5.1}$$

Table 5.3 Simulation Results.

Sintering Temperature	1650 °C	1750 °C
Composite Density (g/cm³)	2.03	2.46
Matrix Porosity (%)	40	3.4
Measured Bending Strength (MPa) [41]	50.75	155.75
Predicted Strength (MPa) – Linear [Error]	47.55 [6.31%]	168.31 [8.07%]
Predicted Strength (MPa) – Quadratic [Error]	50.73 [0.04%]	168.58 [8.24%]

As can be seen, the predictions are in a good agreement with the experimental values reported on the literature, even with considerable simplifications leading to the calculation of matrix porosity and the determination of bulk bending strength. The difference between the linear and quadratic model predictions isn’t negligible and both models provide a good range of predictions, considering the boundary conditions adopted in this case.

5.2 MONTE CARLO SIMULATION RESULTS

5.2.1 Theoretical Tests for ELS

As a way to test the accuracy of the program, some tests were performed to compare its results to the analytical expressions derived by Daniels (eq 2.15).

Test runs with one to five fibers in the bundle were performed and the results were compared to the theoretical predictions based on Daniels' Theory. The fiber input data was as provided from the manufacturer, and as can be seen, both the characteristic strength (σ_0) and Weibull modulus (m) are successfully predicted in these conditions with the Equal Load Sharing algorithm.

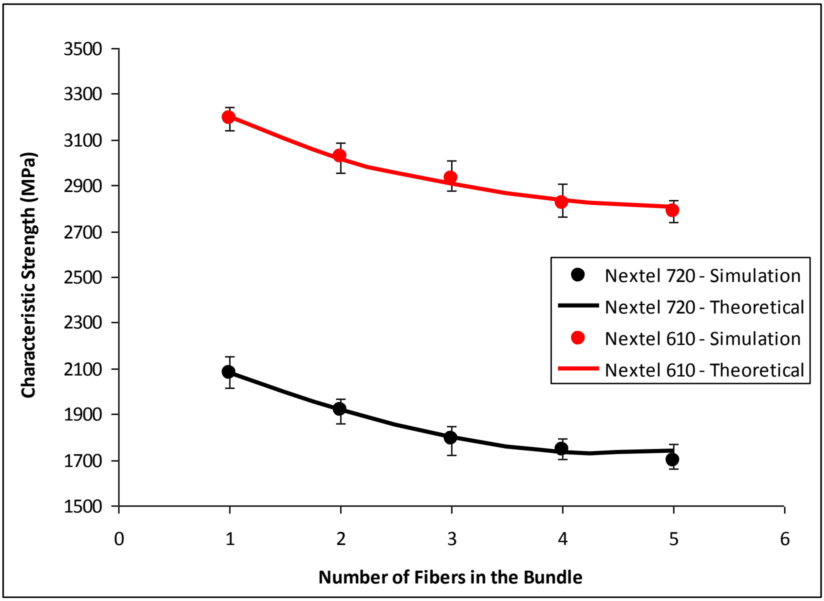

Fig. 5.17 Simulation for ELS, dependence of characteristic strength with increasing number of fibers.

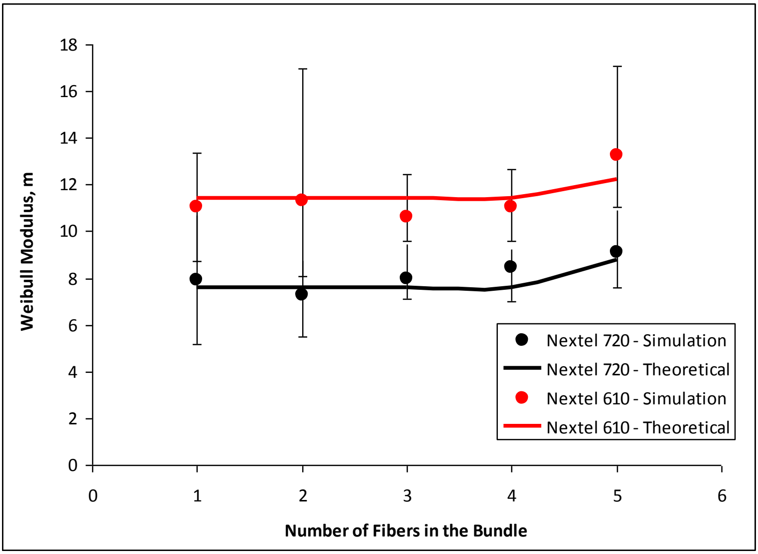

Fig. 5.18 Simulation for ELS, dependence of Weibull modulus with increasing number of fibers.

The test runs were also made with a higher number of fibers in the simulated bundle. The results of the evolution of σ_0 and m with increasing number of fibers are shown in Figs (5.19) and (5.20).

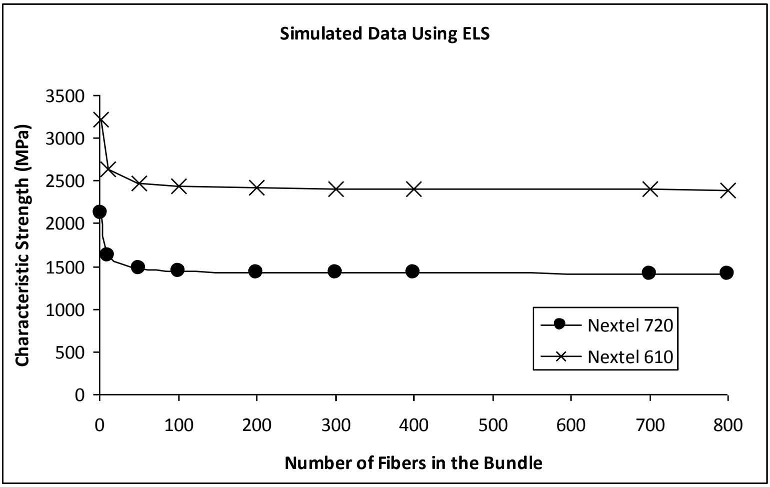

Fig. 5.19 Simulation for ELS, dependence of characteristic strength with increasing number of fibers.

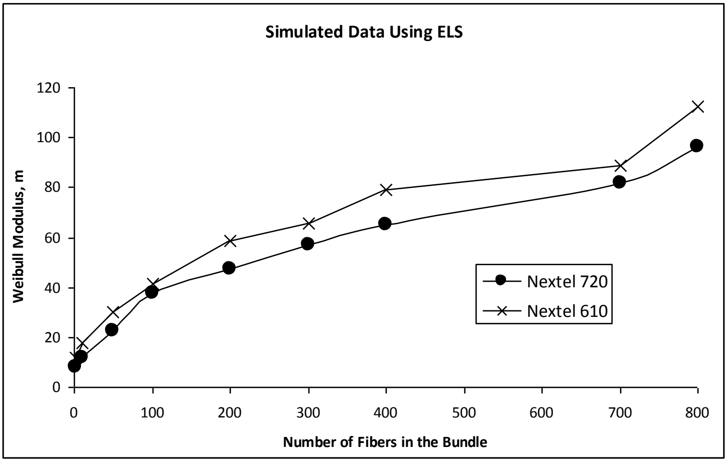

Fig. 5.20 Simulation for ELS, dependence of Weibull modulus with increasing number of fibers.

Note that for an increasing number of fibers in the bundle, the characteristic strength reaches a limit, just as like the equation (2.14), showing that the numerical routine follows the analytical reasoning. One interesting result is in Fig 5.20. It shows that under ELS, the Weibull modulus increases to unrealistic amounts. This shows clearly that even within a dry bundle, the increasing number of fibers also isolate local failures, and the theoretical prediction of ELS are unsuitable for a high number of fibers in the bundle.

5.2.2 Simulation Results for ELS and LLS

Figs. (5.21) and (5.22) show the evolution of the Weibull parameters in the LLS simulations using a Circular LLS rule for the stress intensity factors.

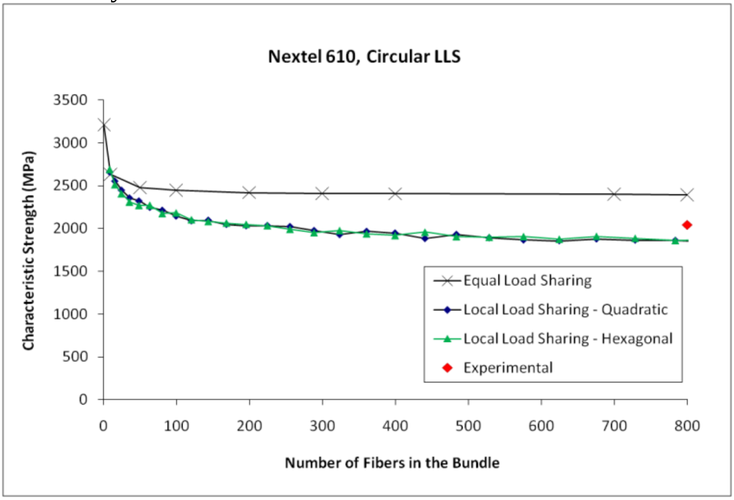

Fig. 5.21 Simulation for LLS, dependence of characteristic strength with increasing number of fibers.

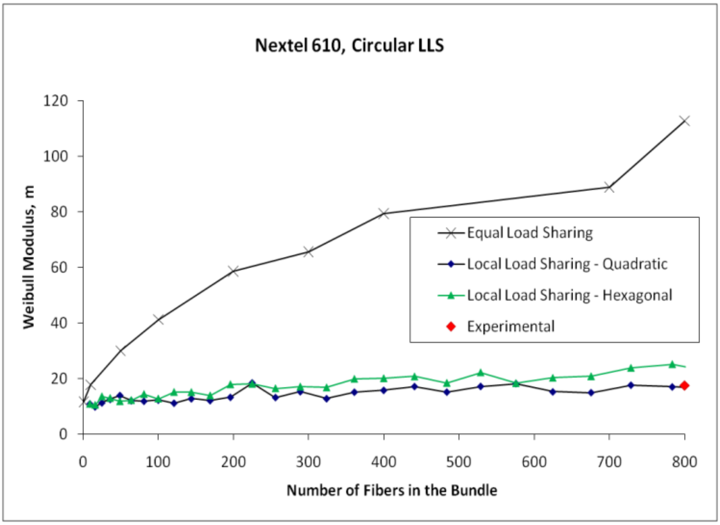

Fig. 5.22 Simulation for ELS, dependence of Weibull modulus with increasing number of fibers.

It can be seen that the LLS theory is more suitable for a bundle with a higher number of fibers, even for dry, desized bundles. One reasonable explanation can be that with the increasing number of fibers, the slippage and friction between the fibers can transmit some part of the overloading locally via shear stress, like the bundles infiltrated with a consolidated matrix.

6 CONCLUDING REMARKS

This thesis developed some models of load transfer between porous matrix and fibers in ceramic matrix composites, concerning short-fiber reinforced composites with a porous matrix, and the mechanical behavior of dry fiber bundles.

An analytical model for short fibers was developed, based on the earlier shear-lag models used for polymeric composites. Moreover, geometry and strength of fibers in addition to the matrix porosity were included in the present analysis. The theoretical curves for the longitudinal and shear stresses distributions along the fiber -porous matrix interface were presented. It became evident that the critical length is governed by the relative properties of the fibers, matrix and porosity, which greatly influenced the load carrying capacity of the fibers in the composites. In addition, the present simplified solution facilitates the understanding of the interface mechanism (shear stress transfer) using porous matrix.

Using data from experiments in the literature, the model was validated, predicting in a successful manner the bending strength of SiC short-fiber reinforced silicon carbide, predicting the influence of the porosity of the matrix.

In addition, a bundle testing algorithm using Monte Carlo Methods was developed. The local-load sharing model results were in a good agreement with the experimental results of single-fiber and bundle testing, showing that for even dry fiber bundles some degree of local load sharing due to friction and slippage. Further development in the model is being made, in order to include factors as damage in the handling of the fibers and slurry infiltration. The model proved flexible and resilient enough to be further complicated.

PUBLICATIONS

SILVA, J. G. P. ; HOTZA, D. ; JANSSEN, R. ; AL-QURESHI, H. A. . Modelling of load transfer between porous matrix and short fibres in ceramic matrix composites. **WIT transactions on engineering sciences (Online)**, v. 72, p. 165-174, 2011.

SILVA, J. G. P. ; AL-QURESHI, H. A. ; HOTZA, D. . Simplified Theoretical Analysis of Short Fibers in Porous Ceramic Matrix. In: 7th International Conference on High Temperature Ceramic Materials and Composites, 2010, Bayreuth. **Proceedings of the 7th International Conference on High Temperature Ceramic Materials and Composites**, 2010. p. 221-227.

GOUSHEGIR, S. M. ; GUGLIELMI, P. O. ; SILVA, J. G. P. ; HABLITZEL, M. P. ; HOTZA, D. ; AL-QURESHI, H. A. ; JANSSEN, R.. Fiber-Matrix Compatibility in an All-Oxide Ceramic Matrix Composite with RBAO Matrix. **Journal of the American Ceramic Society**, 2011 (*accepted*).

REFERENCES

[1] JANSSEN, R., SCHEPPOKAT, S., CLAUSSEN, N., "Tailor-made ceramic-based components - Advantages by reactive processing and advanced shaping techniques", **J. Eur. Ceram. Soc**, 28, 2008, 1369-1379.

[2] CHAWLA, K.K., **Ceramic Matrix Composites.** 1993, London: Chapman & Hall.

[3] GREEN, D.J., **An introduction to the mechanical properties of ceramics**. 1st ed. 1998, Cambridge: Cambridge University Press.

[4] SCHMÜCKER, P.M., ***All-Oxide Ceramic Matrix Composites with Porous Matrices,*** in **Ceramic Matrix Composites, Fiber Reinforced Ceramics and their Applications,** W. Krenkel, Editor. 2008, WILEY-VCH: Weinheim.

[5] MATTONI, M.A, LEVI, C.G., ZOK, F.W., ZAWADA, L.P., *Effects of Combustor Rig Exposure on a Porous-Matrix Oxide Composite.* **Int. J. Applied Ceramic Technology,** 2005. 2(2): p. 133-140.

[6] MATTONI, M.A, LEVI, C.G., ZOK, F.W., ZAWADA, L.P., *Effects of Matrix Porosity on the Mechanical Properties of a Porous-Matrix, All-Oxide Ceramic Composite***. Journal of the American Ceramic Society**, 2001. 84(11): p. 2594-602.

[7] Reinhard A. Simon, a.R.D., *Oxide Fiber Composites with Promising Properties for High-Temperature Structural Applications.* **Advanced Engineering Materials,** 2006. 8(11): p. 1129-1134.

[8] PRITZKOW, W.E.C., *Oxide-Fiber-Reinforced Oxide Ceramics.* **Process Engineering**, 2008. 85(12): p. 31-35.

[9] SIMON, R.A., *Progress in Processing and Performance of Porous-Matrix Oxide/Oxide Composites.* **International Journal of Applied Ceramic Technology**, 2005. 2(2).

[10] WAGNER, F.; **Modellansätze zur Beschreibung der Spannungsverteilung in Faserverbundwerkstoffen.** Seminarvortrag WS 1993/1994 – TUHH

[11] QURESHI, Hazim Ali Al-. **Materiais compostos :** analises e fabricação. 1. ed. Florianópolis: UFSC/CEM, 2010. 469 p. Avaliable in: <http://www.bu.ufsc.br/design/Materiais_Compostos.pdf>

[12] KRENKEL, W. **Ceramic Matrix Composites: Fiber Reinforced Ceramics and their Applications.** Wiley-VCH Verlag GmbH & Co. KGaA, Weinheim: 2008.

[13] NAIR, S.V., e JAKUS, K. (editores). **High Temperature Mechanical Behavior of Ceramic Composites.** Butterworth-Heinemann, Newton, USA: 1995.

[14] LEVI, C.G., YANG, J.Y., DALGLEISH, B.J., ZOK, F.W., EVANS, A.G., "Processing and performance of an all-oxide ceramic composite, " **Journal of the American Ceramic Society**, 81, 1998, 2077-2086.

[15] LANGE, F. F., TU, W. C. e EVANS, A. G. Processing of damage-tolerant, oxidation-resistant ceramic matrix composites by a precursor infiltration and pyrolysis method. **Materials science & engineering. A, Structural materials: properties, microstructure and processing**. 1995, Vol. 195, 1-2, pp. 145-150.

[16] TU, W. C., LANGE, F. F. e EVANS, A. G. Concept for a damage-tolerant ceramic composite with strong interfaces. **Journal of the American Ceramic Society**. 1996, Vol. 79, 2, pp. 417–424.

[17] KRAMB, V. A., JOHN, R. e ZAWADA, L. P. Notched fracture behavior of an oxide/oxide ceramic-matrix composite**. Journal**

of the American Ceramic Society. 1999, Vol. 82, 11, pp. 3087–3096.

[18] KANKA, B. e SCHNEIDER, H. Aluminosilicate fiber/mullite matrix composites with favorable high-temperature properties**. Journal of the European Ceramic Society**. 2000, Vol. 20, 5, pp. 619–623.

[19] ZOK, F. W. Developments in oxide fiber composites. **Journal of the American Ceramic Society.** 2006, Vol. 89, 11, pp. 3309-3324.

[20] ZOK, F. W. e LEVI, G. C. Mechanical Properties of Porous-Matrix Ceramic Composites. **Advanced Engineering Materials**. 2001, Vols. 1-2, 3, pp. 15-23.

[21] KERANS, R. J., et al. Interface design for oxidation-resistant ceramic composites. **Journal of the American Ceramic Society.** 2002, Vol. 85, 11, pp. 2599-2632.

[22] MORGAN, P. E. D., MARSHALL, D. B. e HOUSLEY, R. M. High-temperature stability of monazite-alumina composites. **Materials Science and Engineering A**. 1995, Vol. 195, 1, pp. 215–222.

[23] CHAWLA, K. K., et al. Microstructure and properties of monazite (LaPO4) coated saphikon fiber/alumina matrix composites. **Journal of the European Ceramic Society.** 2000, Vol. 20, 5, pp. 551–559.

[24] KUO, D. H., KRIVEN, W. M. e MACKIN, T. J. Control of Interfacial Properties through Fiber Coatings: Monazite Coatings in Oxide–Oxide Composites. Journal **of the American Ceramic Society.** 1997, Vol. 80, 12, pp. 2987–2996.

[25] BOAKYE, E. E., HAY, R. S. e PETRY, M. D. Continuous Coating of Oxide Fiber Tows Using Liquid Precursors: Monazite Coatings on Nextel 720™. **Journal of the American Ceramic Society.** 1999, Vol. 82, 9, pp. 2321–2331.

[26] HEATHCOTE, J. A., et al. In-plane mechanical properties of an all-oxide ceramic composite. **Journal of the American Ceramic Society**. 1999, Vol. 82, 10, pp. 2721–2730.

[27] FUJITA, H., et al. Mullite/alumina mixtures for use as porous matrixes in oxide fiber composites**. Journal of the American Ceramic Society**. 2004, Vol. 87, 2.

[28] ZAWADA, L. P., et al. Characterization and High-Temperature Mechanical Behavior of an Oxide/Oxide Composite. **Journal of the American Ceramic Society**. 2003, Vol. 86, 6, pp. 981 **-** 990.

[29] HASLAM, J. J., BERROTH, K. E. e LANGE, F. F. Processing and properties of an all-oxide composite with a porous matrix. **Journal of the European Ceramic Society**. 2000, Vol. 20, 5, pp. 607-618.

[30] HE, M. Y., HUTCHINSON, J. W. Crack Deflection at an Interface between Dissimilar Elastic Materials. **International Journal of Solids Structure**. 1989, Vol. 25, 9 pp. 1053-1067.

[31] COX, H.L. The elasticity and strength of paper and other fibrous materials. **British Journal of Applied Physics.** 1952, Vol 3, pp. 72-79.

[32] SCHULTE, K., FIEDLER, B.: **Structure and Properties of Composite Materials**, 2005, TUHH

[33] HARLOW, D.G., PHOENIX, S.L..: The Chain-of-Bundles Probability Model For the Strength of Fibrous Materials I: Analysis and Conjectures. **Journal of Composite Materials,** 1978 vol. 12 no. 2 pp. 195-214

[34] DANIELS, H.E. The Statistical Theory of the Strength of Bundles of Threads. **Proc. Roy. Soc. London A.** 1945, Vol. 183, pp. 405-435.

[35] HEMMER, P.C. et al.: Rupture Processes in Fibre Bundle Model. **Lect. Notes Phys.** 2007, Vol. 705 pp. 27-55.

[36] HORTA-RANGEL et al.: Computer Simulation of Failure Process of a Fiber-reinforced Concrete Composite with Randomly Distributed Fiber Clusters. **Journal of Reinforced Plastics and Composites.** 2008, Vol. 28 n 13 pp. 1613-1624.

[37] HIDALGO et al.: Fracture Model with Variable Range of Interaction. **Physical Review E.** 2002, Vol. 65, 046148 pp. 1-8.

[38] WACHTMAN, J. B. **Mechanical properties of ceramics.** New York: Wiley, 1996.

[39] LARA-CURZIO, E., JENKINS, M.G., Development of test standards for continuous fiber ceramic composites in the United States, **Composites Part A: Applied Science and Manufacturing,** Volume 30, Issue 4, April 1999, Pages 561-567

[40] DASSIOS, K.G., STEEN, M., FILIOU, C., Mechanical properties of alumina Nextel(TM) 720 fibres at room and elevated temperatures: tensile bundle testing, **Materials Science and Engineering A**, Volume 349, Issues 1-2, 25 May 2003, Pages 63-72

[41] QIN, X. H., XIAO, B. L.; DONG, S. M.; JIANG, D. L. SiC_f /SiC composites reinforced by randomly oriented chopped fibers prepared by semi-solid mechanical stirring method and hot pressing **Journal of Materials Science** (2007) Vol. 42 Pages 3488–3494